University of Alberta

Developing General Methods for Studying Enzymatic Reactions at Symmetric Bilayers and Nucleic Acid Triggered Lesion Induced DNA Amplification

by

Yimeng Li

A thesis submitted to the Faculty of Graduate Studies and Research
in partial fulfillment of the requirements for the degree of

Master of Science

Department of Chemistry

Fall 2013
Edmonton, Alberta

Abstract

Understanding molecular recognition is essential to biological and material applications. Surface-specific techniques based on second order nonlinear optical processes such as second harmonic generation (SHG) and sum frequency generation (SFG) are able to selectively study biological events occurring at the interface. We used SFG to probe the Phospholipase D induced hydrolysis reaction of symmetric lipid bilayer supported on a planar silica surface. The $\chi^{(3)}$ SHG technique was used as a complementary technique to monitor the reaction due to changes in interfacial potential of the bilayer after hydrolysis.

Based on our group's previous work, isothermal turnover can be achieved in DNA-templated ligation reactions using destabilizing modifications to the DNA. This system was applied to the detection of target sequences specific to the Hepatitis B virus. The generality of lesion-induced isothermal DNA amplification was also expanded to RNA detection.

Acknowledgements

I wish to give my thanks and respect to Dr. Gibbs-Davis for allowing me the opportunity to work under her guidance as a graduate student and for the wisdom and knowledge she has imparted unto me so that I may successfully complete this project. I would like to mention the collaboration with Dr. Cairo's group that offered help in my research project, specifically to: Chunxia (Cecilia) Zou, Caishun (Carson) Li, and Feng Jia. I would also like to thank the committee examiners for taking the time to read and evaluate this thesis. I thank all my family and friends for all their support throughout my years of study, and my colleagues from the Gibbs-Davis group, thank you for all the kindness in sharing your knowledge and teamwork, especially Dr. Champika Weeraman whose knowledge was essential for me to complete experiments using SFG. It is such a pleasure to work with all of you. I appreciated the support provided by Gareth Lambkin and the Biological Services lab in the Department of Chemistry for help and the available equipment.

Table of Contents

List of Tables

List of Figures

List of Abbreviations

SFG	sum frequency generation
SHG	second harmonic generation
VSFG	vibrational sum frequency generation
DPPC	1,2-Dipalmitoyl-*sn*-glycero-3-phosphocholine
POPC	1-palmitoyl-2-oleoyl-*sn*-glycero-3-phosphocholine
DPPA	1,2-Dipalmitoyl-*sn*-glycero-3-phosphate
PA	phosphatidic acids
DAG	diacyglycerol
PLD	phospholipase D
PLC	phospholipase C
cm^{-1}	wavenumber
ATP	adenosine triphosphate
AMP	adenosine monophosphate
nM	nanomolar
μM	micromolar
pM	picomolar
$^{\circ}C$	degrees Celsius

Chapter 1

Introduction

1.1 Overview

A fundamental question in studying biological systems is how to understand molecular recognition, which is the specific interaction between two or more molecules. For example, molecular recognition involves the specific interactions that occur between receptor and ligand, complementary DNA strands, lipid and protein, etc. The focus of this thesis aimed at understanding such interactions, which can be divided into two parts: (1) monitoring membrane-enzyme interactions and (2) developing enzyme-induced DNA amplification.

Many molecular interactions take place on biological membranes; therefore many researchers have shown interest in understanding the mechanism of these interactions. Various techniques can be used to probe biological events that occur on membranes. The focus of the first research project is to study membrane-enzyme interactions, more specifically, the interactions of phospholipase D on a phospholipid membrane. Due to the complexity of the biological membrane, I aim to investigate the interaction of phospholipase D on membranes using a biological model. This model allows for monitoring membrane structure changes during the hydrolysis processes spectroscopically using sum frequency generation (SFG) and second harmonic generation (SHG).

Rapid and reliable sequence-specific nucleic acid detection is important for disease detection, food inspection, etc. The second research project is dedicated to expanding a method of isothermal DNA-self replication and detection based on previous work in the Gibbs-Davis group, which involves selective recognition of particular base sequences by synthetically modified DNA

probes. DNA self-replication or amplification in this system can be achieved by DNA-templated ligation reactions using destabilizing modifications to the DNA. The goal in this research is to find a general system to amplify and detect a target sequence specific to the Hepatitis B virus. Using a similar approach, we extend the application to RNA detection.

1.2 Cell membranes and its components

The cell membrane plays an important role in many biological processes of cells. It consists of a large number of lipids, proteins and a relatively smaller amount of carbohydrates (Figure 1.1A).[1] The most abundant lipids in most membranes are phospholipids, which are amphipathic molecules with a hydrophilic, polar head group and a hydrophobic, nonpolar tail (Figure 1.1B). They assemble into a lipid bilayer that orients the polar head group towards the aqueous media and the hydrophobic tails project towards the bilayer interior.[1] Phospholipids not only define the shape and the structure of a cell, but also act as a platform to exchange information between the intracellular and the surrounding environment. These processes often involve a variety of proteins and carbohydrates embedded in or associated with the cell membrane (Figure 1.1A). Due to the complexity of living cells, these mechanisms of the biological interactions and processes are hard to monitor *in vivo* at the membrane. Therefore, model membranes *in vitro* are used to study these biological processes.

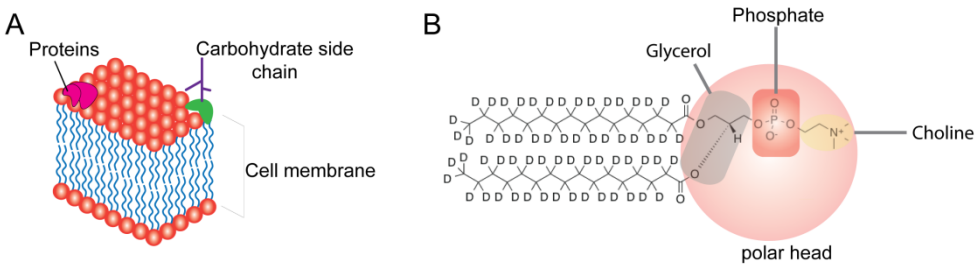

Figure 1.1 The components of the cell membrane. (A) The cell membrane is made up of a phospholipid bilayer with various proteins and carbohydrates side chains embedded in or associated with the membrane. (B) The polar head of a phospholipid (DPPC-d_{62}) consists of a choline, a phosphate group and a glycerol backbone.

1.3 Biophysical studies of lipid bilayers

There are different techniques that have been used to investigate lipid bilayers and model membranes. For example, atomic force microscopy (AFM) allows for probing the surface to study the ordering of membrane-bound proteins.[2] Surface plasmon resonance spectroscopy (SPR) and complementary techniques are very sensitive to protein/peptide binding to the membrane.[3] Spectroscopic measurements that focus on the lipid structure directly provide more structural information and a better understanding of the molecular interactions. For example, polarization modulation external infrared reflection absorption spectroscopy (PM-IRRAS) studies offer vibrational information about the membrane proteins and peptides.[4] However, the drawback of this technique is the lack of surface specificity, which allows other species in the aqueous layer to interfere with the measurement. Surface-specific techniques based on second order nonlinear optical processes such as second harmonic generation (SHG) and sum frequency generation (SFG) overcome the main drawbacks of conventional

linear optical techniques in terms of interface selectivity and sensitivity. Consequently, they are able to selectively study events occurring at the interface.[5,6,7]

1.4 Synthesis of model membranes

Planar supported lipid bilayers (PSLBs) on glass, silica, mica, polymer films or other inorganic surfaces are widely utilized to mimic many aspects of cell membrane behavior as biological models.[8,9] These PSLBs have been used to study a variety of fundamental biological processes on membranes, including membrane structures, asymmetry, orientation, dynamics and interactions with proteins, peptides and small molecules.[4,10] PSLBs are typically formed through two different methods, Langmuir-Blodgett/Langmuir-Schaefer (LB/LS) technique or vesicle fusion. In the LB/LS technique, first lipids are spread at an air/water interface to form a lipid monolayer. The first leaflet of the bilayer on the substrate can then be deposited by withdrawing a hydrophilic substrate from the aqueous monolayer though the air/water interface, resulting in a hydrophobic monolayer in a vertical orientation to the substrate (LB deposition) with the polar head groups oriented towards the surface. The second leaflet is added by horizontally pushing the monolayer-coated surface through another Langmuir-Blodgett film consisting of the same or different lipid (LS deposition) (Figure 1.2A).[11,12]

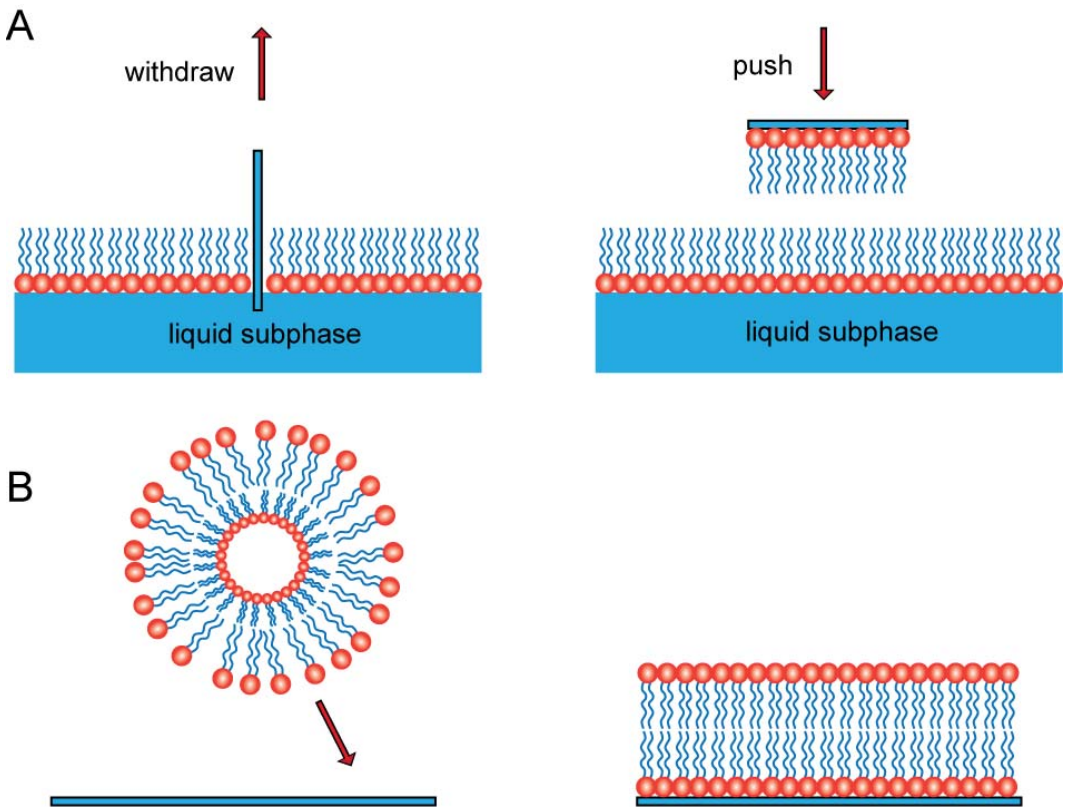

Figure 1.2 The most common techniques for the formation of planar supported lipid bilayers. (A) The Langmuir-Blodgett /Langmuir-Schaefer (LB/LS) technique: the PSLBs is achieved by pulling the hydrophilic substrate vertically through a Langmuir-Blodgett lipid monolayer followed by pushing the substrate horizontally through another lipid monolayer. (B) The vesicle fusion technique: a solution of vesicles adsorb and fuse to the hydrophilic substrate spontaneously.

The LB/LS technique is particularly well studied for forming asymmetric bilayers where the bottom and top leaflet consist of different lipids. However, asymmetric lipid bilayers with single or two different lipid components can only be examined below their main phase transition temperature (T_m), as the asymmetric lipid bilayer will rapidly undergo flip-flop (translocate both laterally and across the membrane) when the temperature is near or above the main phase transition temperature.[13] For this reason, the temperature must be rigorously controlled; otherwise, it limits the selection of the lipids on the planar surface.

The vesicle fusion technique is another technique that can be used to prepare symmetric bilayers and has the advantage of a simpler protocol than the LB/LS method. In vesicle fusion, vesicles, or liposomes, dispersed in solution first adsorb to the surface, fuse with each other leading to an increase in radius, and then rupture and spread on the surface, assembling into a lipid bilayer. Through continual spreading, small bilayer patches can form a large and continuous bilayer (Figure 1.2B).[14,15] In this thesis, the vesicle fusion method was used to conduct all the studies described in Chapter 2.

1.5 Introduction of non-linear optical spectroscopy

Surface-specific techniques based on second order nonlinear optical processes such as second harmonic generation (SHG) and sum frequency generation (SFG) are able to selectively study events occurring at the interface[5,6,7]. In recent studies, researchers applied SHG and SFG techniques to study biological processes at the surface and buried interfaces *in situ.*[16,17,18,19,20,21]

1.5.1 The theory of second harmonic generation

SHG studies can be used to study virtually any biological molecule at an interface by introducing a second-harmonic-active probe or taking of advantage of intrinsic properties of the assembled biomolecules.[17,22,23] Within the electric dipole approximation, which assumes that the magnetic-dipole and other contributions to the nonlinearity are negligible under this assumption, SHG does not occur in a centrosymmetric medium such as bulk water SHG does not occur

because of inversion symmetry. However, SHG can be obtained from the interface of two centrosymmetric media, such as the interface of water and fused silica, due to the break in inversion symmetry.[24] SHG is a coherent optical process that occurs when light interacts with the oriented dipoles in the material. The dipoles interact with the applied electric field of frequency ω, resulting in an induced polarization that oscillates at frequency 2ω ($P_{2\omega}$). This oscillating polarization results in a new electric field ($E_{2\omega}$), which emanates coherently from the interface with twice the incident frequency and half the incident wavelength.

The SHG intensity I_{SHG} depends on the incident electric field (E_{ω}) and the second-order susceptibility $\chi^{(2)}$, which is generally very small for most interfacial systems.

$$\sqrt{I_{\mathrm{SHG}}} = E_{\mathrm{SHG}} \propto P_{2\omega} = \chi^{(2)} E_{\omega} E_{\omega} \tag{1.1}$$

$\chi^{(2)}$ can be broken up into a resonant ($\chi_{\mathrm{R}}^{(2)}$) and a nonresonant ($\chi_{\mathrm{NR}}^{(2)}$) term as

$$E_{\mathrm{SHG}} \propto \sqrt{|\chi^{(2)}|^2} = \sqrt{\left|\chi_{\mathrm{R}}^{(2)} + \chi_{\mathrm{NR}}^{(2)} \mathrm{e}^{\mathrm{i}\Delta_{\emptyset}}\right|^2} \tag{1.2}$$

the resonant and non-resonant terms can be linked through a phase factor $\Delta_{\emptyset}$.[18,25] For the silica/water interface, the phase difference of these two terms is assigned 90°. The resonant term of the second-order susceptibility can be expressed as:

$$\chi_{\mathrm{R}}^{(2)} = N_{\mathrm{ads}} \langle \beta^{(2)} \rangle \tag{1.3}$$

N is the number density of molecules that are adsorbed on the surface which are in resonance and $\beta^{(2)}$ is the second order molecular hyperpolarizability averaged over all molecular orientations. This molecular hyperpolarizability can be expressed as:

$$\beta^{(2)} \propto \frac{A}{\omega_{ca} - 2\omega + i\Gamma} \quad (1.4)$$

A is the oscillator strength, ω_{ca} is the resonant frequency of a particular electronic excitation from a molecule and Γ is a dampening term. SHG is greatly enhanced by resonance effects when the second harmonic frequency (2ω) approaches that of a molecular electronic transition (ω_{ca}). Resonantly enhanced SHG allows for specific interfacial molecules to be selectively probed without requiring labels if the molecular hyperpolarizability is relatively large and the molecules are ordered at the interface resulting in a net orientation.

To illustrate, resonant SHG can be used to detect the presence of bound proteins or lipids to a lipid membrane if the protein or lipid has electronic transitions at the frequency of the SHG light. As an example, a comparison of the binding properties of avidin, streptavidin, neutrAvidin, and antibiotin antibody was studied using this method at a biotinylated lipid bilayer.[26] SHG has also been used for measuring melittin binding to the supported lipid bilayer.[27]

In addition to the contribution from $\chi^{(2)}$, I_{SHG} is also modulated by the presence of a third static electric field arising from surface charge, which is described by the third-order susceptibility, $\chi^{(3)}$. Overall, the I_{SHG} from the interface can be expressed as :

$$\sqrt{I_{SHG}} = E_{SHG} \propto P_{2\omega} = \chi^{(2)} E_\omega E_\omega + \chi^{(3)} E_\omega E_\omega \Phi \quad (1.5)$$

In this expression, E_{SHG} is the SHG electric field, E_ω is the electric field of the incoming light at the frequency ω, $\chi^{(2)}$ and $\chi^{(3)}$ are the second- and third-order nonlinear susceptibilities of the interface, respectively and Φ is the interfacial potential that depends on the surface charge density.[16,28] It follows from equation

1.5 that the I_{SHG} will be changed by changing the interfacial potential, Φ. Monitoring the changes of SHG signal that directly arise from interface potential changes is called the Eisenthal $\chi^{(3)}$ technique. At an insulator surface like silica, the interfacial potential is altered by screening the surface charges or varying the surface charge density. Consequently, the $\chi^{(3)}$ technique is a useful method for studying electrostatic interactions and reactions that generate charges at the buried silica/water interface.[22,23,29] Unlike resonantly enhanced SHG, there are only limited examples of studying lipid bilayers using the $\chi^{(3)}$ technique to study the transmembrane movement of ions.[28,30]

1.5.2 The theory of vibrational sum frequency spectroscopy

The same argument about interface specificity and sensitivity can be applied to the case of vibrational sum frequency generation (VSFG), which is also a second-order nonlinear optical spectroscopy that requires lack of inversion symmetry under the electric dipole approximation. As the bulk aqueous phase is isotropic, with a random distribution of molecules and their corresponding transition dipoles, it will generate no or very little signal. In contrast, inversion symmetry is broken at the interface of the aqueous phase and air or solid surfaces; therefore, SFG signal is generated. VSFG spectroscopy has led to novel applications that provide information on enzymatic reactions on phospholipid bilayers as well as transmembrane dynamics. In SFG, two photons of IR and

visible frequency are overlapped in space and time on the sample surface to generate one photon at the sum frequency as shown:

$$\omega_{\mathrm{sum}} = \omega_{\mathrm{vis}} + \omega_{\mathrm{IR}} \tag{1.6}$$

The resulting SFG intensity (I_{SHG}) reflected from the interface is proportional to the square modulus of the surface second-order nonlinear susceptibility, $\chi^{(2)}$, as shown:

$$I_{\mathrm{SFG}} \propto \left|\chi^{(2)}\right|^2 \propto \left|\chi_{\mathrm{NR}}^{(2)} + \sum_{\upsilon} \chi_{\upsilon}^{(2)}\right|^2 \tag{1.7}$$

where $\chi^{(2)}$ consists of a sum of resonance terms and a nonresonant term ($\chi_{\mathrm{NR}}^{(2)}$). The resonant macroscopic nonlinear susceptibility, $\chi_{\upsilon}^{(2)}$, is related to ω_{IR}, the frequency of the incident infrared beam:

$$\chi_{\upsilon}^{(2)} \propto \frac{\mathrm{A}_{\upsilon}}{\omega_{\mathrm{IR}} - \omega_{\upsilon} + \mathrm{i}\Gamma_{\upsilon}} \tag{1.8}$$

where A_{υ} is the strength of the oscillator whose amplitude is nonzero when the raman and the infrared transitions are both spectroscopically allowed. ω_{υ} is the frequency of the vibrational mode, and Γ_{υ} is the line width of the transition. When the infrared pulse has its frequency tuned to match the vibrational frequency of molecules at the surface, a vibrational spectrum can be provided from the interface due to the resonantly enhanced SFG signal.[17,31] Specifically, $\chi^{(2)}$ is greatly enhanced by resonance effects when the incident infrared frequency (ω_{IR}) approaches ω_{υ}, therefore an SFG intensity enhancement is observed.

Like SHG, SFG requires a net orientation of molecules at the interface being probed; the relative arrangement of each layer of the lipid bilayer will have an effect on the sum frequency signal. For a perfectly symmetric, lipid bilayer, the

orientation of the inner and outer layer of the lipid will result in second order susceptibilities of opposite sign or phase from each other. Thus, the SFG signal will destructively interfere, leading to cancellation of the net sum frequency signal.

1.5.3 Applications of vibrational sum frequency generation spectroscopy in studying cell membranes

Interface studies have been advancing rapidly with advances in interface specific nonlinear optical techniques. During the past decade, SFG has been successfully applied to study lipids, proteins, peptides, and other biological molecules at interfaces.[32,33] In particular, people have applied SFG to study the interactions between peptides/proteins and lipid bilayers. The structure and kinetic results from these studies can provide molecular level information.

In one example, Conboy and coworkers used SFG to show one of the most important aspects of the behavior of lipids in cell membranes: their ability to translocate across the membrane (flip-flop). Beginning with an asymmetric lipid bilayer consisting of a protonated leaflet and a deuterated leaflet, they observed the transbilayer movement of the phospholipids based on changes in SFG intensity as a function of time at different temperatures.[31] Later in 2007, they successfully demonstrated that the introduction of gramicidin A led to rapid flip-flop of the DSPC/DSPC-d_{83} bilayer with SFG.[32] In related work, by directly observing SFG from the lipids in the bilayer, Chen and co-worker studied their conformation after interacting with antimicrobial peptides; the peptide's SFG signal was also investigated mode during the interaction.[33]

1.6 Using the $\chi^{(3)}$ SHG technique and vibrational SFG to study the reaction of phospholipase D and C with symmetric phospholipid bilayers

Most of the previous SFG studies investigated the lipid bilayers by monitoring the symmetric C-H stretching mode of methyl groups from the acyl chain in asymmetric lipid bilayers. In contrast, in Chapter 2, we investigate phospholipase-induced hydrolysis processes at symmetric lipid bilayers using the methyl signals from the lipid head group as an indicator of lipid order and movement. We also monitor this hydrolysis process by observing the interfacial potential changes at the membrane surface using the SHG $\chi^{(3)}$ method.

1.7 Overview of nucleic acids

1.7.1 Introduction to DNA and RNA

DNA, or deoxyribonucleic acid, was discovered in the mid-1880s by Johann Friedrich Miescher. DNA is the primary molecule for storing information and instructions to allow an organism to survive. Not until a century later, its significance in life process was recognized as being responsible for carrying genetic instructions for the development and functioning of all known living organisms as well as many viruses.[34] Genomic DNA exists as a double helix in which two complementary strands with the opposite direction (anti-parallel) are held together by hydrogen bonds between base pairs and hydrophobic interactions between the two strands. Each DNA strand is a high molecular weight polymer of nucleotides that consist of a sugar backbone (deoxyribose), a phosphate and a nucleobase. The four nucleobases can be divided into two classes: the purine

bases include adenine (A) and guanine (G), and the pyrimidine bases cytosine (C) and thymine (T) as depicted in Figure 1.3. Base A always pairs with base T through two hydrogen bonds and base C with base G through three hydrogen bonds. The complementary bases form a hydrophobic interior, while the sugar phosphate backbone is hydrophilic and allows the DNA to be water soluble at the same time protecting the interior nucleobases from media. Owing to the stability of the deoxyribose functional group and protected nucleobases, the duplex structure of DNA can help store tremendous amounts of genetic information.

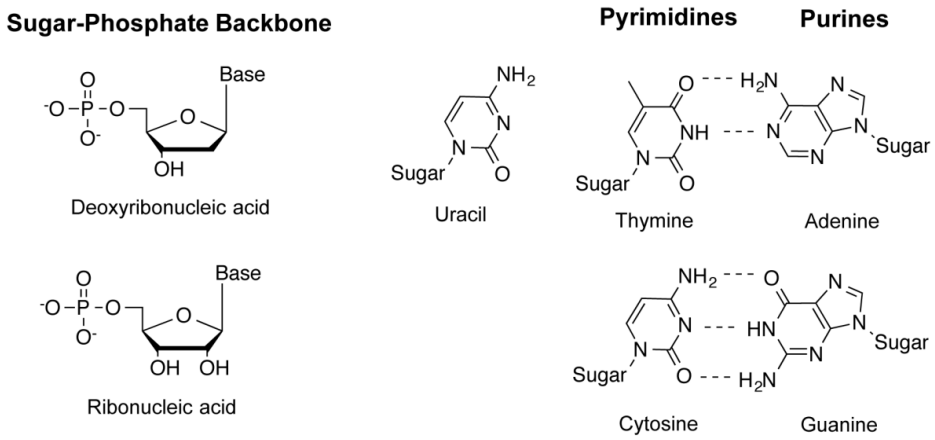

Figure 1.3 Chemical structures of nucleobases found in DNA, RNA, sugar backbone, and phosphate group.

Related to DNA, ribonucleic acids (RNA) are present as short-term information-storing molecules. RNA is composed of a ribose sugar in place of the deoxyribose sugar in DNA. Additionally, RNA contains uracil (U) in place of thymine to pair with adenine. In contrast to the structure of DNA, RNA exists as a single strand and not a helix; the single strand of RNA can form loops by intra-strand base pairing to self-complementary regions in the RNA.[35]

1.7.2 The biological role of DNA and RNA

A gene is the basic unit of heredity of living organisms, which consists of a sequence of ordered DNA nucleotides at a given location on a given chromosome that provides instructions on how to make a specific protein or enzyme. Crick first proposed the central dogma of molecular biology, a theory that describes how information is coded by DNA molecules and transcribed to RNA molecules, and then translated to proteins.[36] DNA is responsible for long-term genetic information storage, whereas RNA is a short time carrier, which helps regulate the amount of protein and enzyme produced. Information can only pass from nucleic acid to nucleic acid or to protein, but can not be transferred from protein to protein or nucleic acid. Thus, an organism can grow by making more proteins through transcription and translation of the DNA. In order for an organism to grow its cells must reproduce, which means that it also needs to replicate its DNA, so that each cell has the same genetic information.

During DNA replication, the enzyme DNA helicase is used to unwind the DNA helix, which allows both strands to serve as templates; the 3' DNA strand is called the leading strand, and 5' DNA strand is named the lagging strand. DNA primases attach to both strands of the unwound DNA helix and act as the start positions for DNA replication. A polymerase enzyme replicates the DNA in the 3' to 5' direction in both the template and lagging strands. The replicated DNA on the leading strand is continuous, whereas the DNA replicated on the lagging strand is broken into fragments called Okazaki fragments. The Okazaki fragments are later combined to form one continuous DNA strand by DNA ligase. This

process continues until the end of the chromosome.[37]

The genomic DNA contains all of the genetic information of the organism, yet proteins are synthesized only as needed. This selective expression of genes stems from the selective transcription of the DNA sequence encoding a gene to its RNA complement. With the help of proteins called transcription factors that select the particular sequence to be replicated and other proteins that separate the DNA duplex, the DNA is transcribed to a single strand messenger RNA (mRNA) by RNA polymerase. In eukaryotic cells, the mRNA travels out of the nucleus of the cell and into the cytoplasm. Here, the mRNA is "read" and the protein is synthesized with the help of ribosomes and transfer RNA. Specifically, the ribosome reads the mRNA sequence in groups of three, called codons, which code for a specific amino acid. The ribosome recruits tRNA molecules that contain the complementary codon to the mRNA at one end and an amino acid at the other end. The ribosome then catalyzes the formation of a peptide bond between two amino acids on neighboring tRNA molecules. This process continues until the end of the mRNA is reached.

1.8 Current DNA and RNA detection methods

The nucleic acid sequence present in each cell is unique to that specific organism. Consequently the nucleic acids found in bacteria, viruses, and pathogens offer unique targets for the identification and diagnosis of many diseases. Moreover, sequence-selective DNA detection is essential to unravel the

genetic basis of diseases and could potentially be employed in preventative health care, early disease diagnosis and drug treatment of specific human diseases.[38,39,40,41] Such methods could also be used as tools for DNA detection in food samples to assure accuracy on food labeling, safety and quality of food.[42,43,44]

1.8.1 The common strategies for DNA detection

In most cases, a very low concentration of the target sequence is present in the sample, which makes positive target detection problematic. As a significant amount of target DNA is essential for analyses, methods for sequence amplification in detection have been widely studied.[45,46,47] The most prevalent amplification method is the polymerase chain reaction (PCR), which exponentially amplifies a specific DNA target sequence *in vitro* with extremely high sensitivity. PCR amplification can be achieved from two small DNA primers that contain complementary sequences to the DNA target sequence. The DNA target can then be amplified through a cycle involving heat denaturation of the DNA target resulting in two complementary single-strand DNA templates, annealing of the primers to their complementary sequences on these templates, and extension of the annealed primers with DNA polymerase to form complements to the original DNA target strands.[48] This thermal cycle is repeated to achieve exponential amplification since all strands, including those newly formed, are amplified at once. With the high specificity for the DNA target, PCR technology has become a very powerful tool for diagnosis of specific infectious

diseases, including pathogen HIV-1[49,50], hepatitis B and C virus[51] and mycobacterium tuberculosis[52,53] and genetic diseases stemming from specific mutations. [54,55]

However, the sensitivity of PCR is also its major drawback, since a very small amount of contaminating DNA in the sample could also be amplified; this leads to a relatively low specificity. Research groups have studied the impact of parasitic sequences to overwhelm the original target sequence.[56] Also PCR requires thermal cycling instrumentation, and usually considerable operator expertise, thus limiting its use to highly sophisticated facilities. Therefore, a technique with high specificity, low cost, easy and portable use, is needed. Consequently, isothermal DNA amplification methods have been developed as an alternative to PCR-based amplification for point-of care diagnostics.

1.8.2 Isothermal amplification methods

Since the early 1990s, researchers started to draw attention to isothermal DNA amplification for point-of care diagnosis. The major DNA-based isothermal amplification methods in diagnosis include: strand-displacement amplification (SDA)[57,58], rolling circle amplification (RCA)[59] and helicase-dependent amplification (HDA)[60] and transcription mediated amplification (TMA)[61]. Each of these techniques is innovative in its method to amplify a DNA target under isothermal conditions. Techniques such as SDA, LCR and TMA are approved by the FDA and are now commercially available in diagnostic kits for the detection of microbial infections.[62] Two particularly attractive methods for point-of-care

diagnostics are RCA and loop-mediated isothermal amplification, a form of SDA, which will be further elaborated on.

1.8.2.1 Strand-displacement amplification: Loop-mediated isothermal amplification

Among all the isothermal DNA amplification methods, loop-mediated isothermal amplification (LAMP) is one of the most widely used SDA-based amplification techniques for its high specificity, efficiency and rapid pathogen detection at a constant temperature.[47] Four specially designed primers are used that recognize six distinct DNA sequences on the target DNA (Figure 1.4). One of the inner primers anneals to the complementary sequence of the target DNA and extends the annealed primer with DNA polymerase, which facilitates displacement and release of the complementary DNA strand (Figure 1.5A). (*Bacillus stearothermophilus* DNA polymerase lacks 5'-3'exonuclease activity and is functional for strand displacement). The outer primer then anneals to the target DNA and is elongated by DNA polymerase releasing the newly synthesized DNA strand (Figure 1.5B and C). The displaced strand in Figure 1.5B forms a loop stem structure because of the complementarity of F_1 and F_{1C} (Figure 1.5E), and it serves as a template for the reverse inner primer extension. The outer primer then binds to displace the elongated inner primer strand, which releases a double stem loop structure strand (Figure 1.5G) that has the sequence and its complement on either sides of the strand (F_1 bind to F_{1C}, B_1 bind to B_{1c}). This serves as the starting material for continuing replication using the backwards and

forwards inner primers to form a flower-like structure long-chain DNA product. By introducing extra loop primers, LAMP amplification can be improved by increasing the number of starting points for DNA synthesis for a faster readout.[63] With the addition of reverse transcriptase, this method is able to detect RNA target sequences by transcribing them to DNA followed by amplification (RT-LAMP).

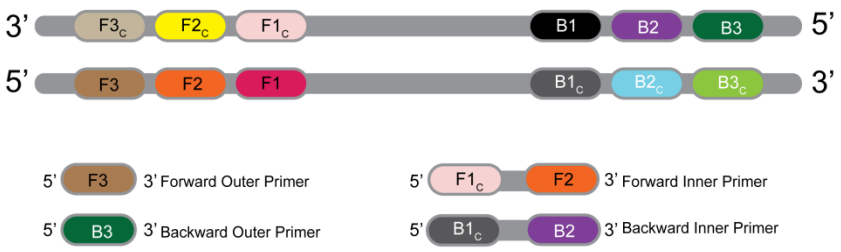

Figure 1.4 Schematic representation of the primer design for the LAMP assay. The four specially designed primers are: two inner primers which contain sequences of the sense and antisense strands of the target DNA and consequently form a loop after elongation and two outer primers that are complementary to the target DNA.

Through the amplification process, pyrophosphate ions are produced (1.9), which bind to magnesium ions forming magnesium pyrophosphate ($Mg_2P_2O_7$), which is a white precipitate (1.10). Therefore, amplification can then be monitored by measuring the turbidity.[64] Alternative detection methods involve agarose gel analysis or real-time detection through fluorescence analysis.[65] The disadvantage of LAMP, however, is the complicated primer design and laboratory based analysis. The advantage is rapidity, high specificity, 10 to 100 fold more sensitivity than PCR with easy detection (visualize turbidity by the naked eye).

$$(DNA)_{n-1} + dNTP \rightarrow (DNA)_n + P_2O_7^{4-} \quad (1.9)$$

$$P_2O_7^{4-} + 2Mg^{2+} \rightarrow Mg_2P_2O_7 \quad (1.10)$$

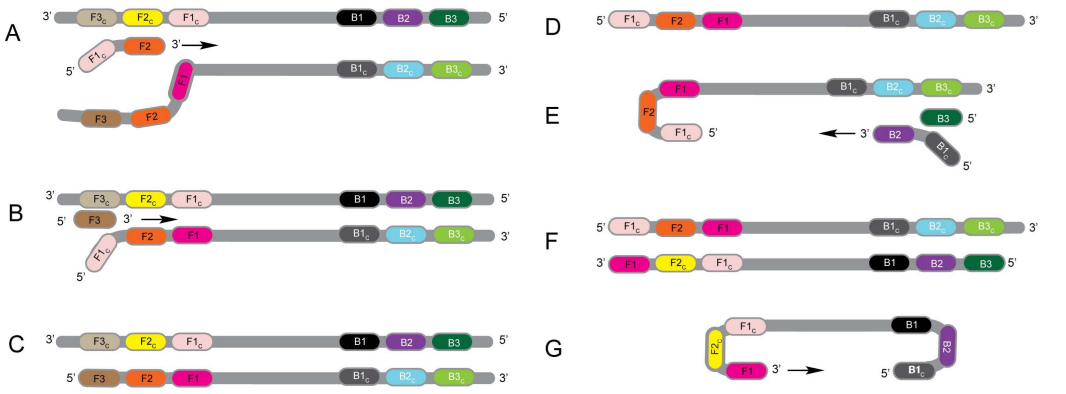

Figure 1.5 An illustration of the first steps of LAMP amplification. (A) The forward inner primer anneals to the DNA template and is elongated. (B) The forward outer primer (F3) binds to the target. As it is elongated it displaces the elongated inner primer. (C) The double stranded DNA formed from the F3 primer. (D-E) The displaced single stranded DNA from B forms a loop and hybridizes to the backwards inner primer, which is elongated. Next the backwards outer primer binds and displaces the elongated inner primer resulting in a duplex (F). (G) The displaced inner primer forms a double loop that is amplified through a series of steps by the two inner primers.

1.8.2.2 Rolling circle amplification

Rolling circle amplification (RCA) is another isothermal amplification strategy that has been widely employed in DNA-based amplification. RCA has been used with high sensitivity and specificity in the detection of single nucleotide polymorphisms (SNP) and allows for multiplexing. RCA has been applied in the analysis of nucleic acids by coupling with electrochemistry[66], chemiluminescence[67] and colorimetry[39,68] methods for detection. In brief, a short DNA primer is introduced to hybridize with a circular single–stranded DNA target. The primer is extended along the circle by DNA polymerase generating a

copy of complementary of single-stranded DNA (Figure 1.6A). The commonly used polymerase in RCA is Phi29 DNA polymerase.[60] Phi29 has a relatively high processivity, and has the function of strand displacement. This copied DNA that is complementary to the circular DNA target is displaced from the target by the polymerase allowing for continuous amplification of the target until the polymerase and reagents are exhausted. This process eventually generates a long single-stranded DNA with multiple copies complementary to the circular target DNA (Figure 1.6A). The smaller the circular target size, the more efficient the amplification as more copies of the target DNA are obtained in a given time with less chance for strand breakage.[64] In order to enhance amplification, another form of RCA called multiple primed rolling circle amplification can be used. In this process multiple primers are introduced that anneal to the circular DNA target (Figure 1.6B), causing amplification to start at multiple locations on the circular target. Combining SDA designed primers that include the sequence of the target DNA with RCA can achieve even more sensitive detection.[69]

A linear DNA can also be detected and amplified through the RCA method using a padlock probe design (Figure 1.6C). A padlock probe has two segments that have sequences complementary to the single-strand DNA target. In the presence of DNA target, the padlock probe hybridizes to the DNA target and the nick is sealed by DNA ligation resulting in a circularized padlock probe. The circularized probe then acts as a template in the RCA process.[68] The RCA detection assay achieves good specificity with the specific circular padlock probes. However, the sensitivity is low in the target-primed RCA reaction, since

one target only generates one circular padlock probe, resulting in linear amplification.[70]

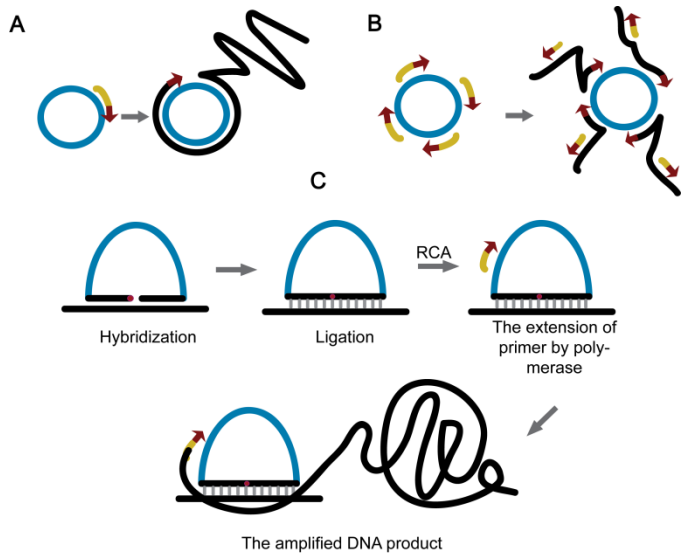

Figure 1.6 Schematic representation of rolling circle amplification: (A) Target specific rolling circle amplification. (B) Multiple primed rolling circle amplification. (C) The padlock primed rolling circle amplification: the primer hybridizes to the single-strand DNA target stand, followed by ligation at the nick site and RCA.

1.9 The significance of isothermal detection

As discussed, methods for amplifying nucleic acids are very valuable for the detection and quantification of specific nucleic acid sequences. Such amplification methods can also be used to detect other targets, including proteins, ligands, and small molecules.[71] In the past decade, more and more researchers have tried to develop or optimize isothermal amplification strategies and couple them with different detection methods for point-of-care diagnostics. Assays using SDA have been approved by the Food and Drug Administration (FDA) and are now commercially available as diagnostic kits for the detection of microbial

infections.[72,73] Although these isothermal amplification developments have many advantages, they also have some limitations. For example, LAMP requires holding the reaction at an elevated temperature, which makes it rather expensive for point-of-care diagnostics. Moreover, it does not work on all targets. For padlock primed RCA assay, the sensitive is relatively low without coupling with other detection methods, which makes it hard for detecting lower concentration target in a simple way. Consequently, new isothermal methods are needed that operate near room temperature for simple and rapid detection.

1.10 Finding the generality of isothermal DNA self-replication induced by destabilizing lesion and expanding it to a RNA system.

Our group has successfully established an isothermal DNA self-replication system by using destabilizing modifications to the DNA. In Chapter 3, we aim to find the generality of this system to detect a sequence that is specific to Hepatitis B virus. The simplicity and generality of this DNA amplification method are also used to develop a RNA detection system.

1.11 Reference

1. Ouellette, R. J., *Organic Chemistry*. Second ed.; Prentice hall: upper saddle river, New jersey 07458, p 380-382.

2. Milhiet, P. E.; Giocondi, M. C.; Baghdadi, O.; Ronzon, F.; Roux, B.; Le Grimellec, C., *Embo Rep.* **2002,** *3* (5), 485-490.

3. Devanathan, S.; Salamon, Z.; Lindblom, G.; Grobner, G.; Tollin, G., *FEBS J.* **2006,** *273* (7), 1389-1402.

4. Estrela-Lopis, I.; Brezesinski, G.; Mohwald, H., *Biophys. J.* **2001,** *80* (2), 749-754.

5. Shen, Y. R., *Annu. Rev. Phys. Chem.* **1989,** *40*, 327-350.

6. Richmond, G. L.; Robinson, J. M.; Shannon, V. L., *Prog. Surf. Sci.* **1988,** *28* (1), 1-70.

7. Corn, R. M.; Higgins, D. A., *Chem. Rev.* **1994,** *94* (1), 107-125.

8. Castellana, E. T.; Cremer, P. S., *Surf. Sci. Rep.* **2006,** *61* (10), 429-444.

9. Tien, H. T.; Barish, R. H.; Gu, L. Q.; Ottova, A. L., *Anal. Sci.* **1998,** *14* (1), 3-18.

10. He, Q.; Li, J. B., *Adv. Colloid Interface Sci.* **2007,** *131* (1-2), 91-98.

11. Liu, J.; Conboy, J. C., *Langmuir* **2005,** *21* (20), 9091-9097.

12. Brosseau, C. L.; Leitch, J.; Bin, X.; Chen, M.; Roscoe, S. G.; Lipkowski, J., *Langmuir* **2008,** *24* (22), 13058-13067.

13. Richter, R. P.; Berat, R.; Brisson, A. R., *Langmuir* **2006,** *22* (8), 3497-3505.

14. Anderson, T. H.; Min, Y. J.; Weirich, K. L.; Zeng, H. B.; Fygenson, D.; Israelachvili, J. N., *Langmuir* **2009,** *25* (12), 6997-7005.

15. Shen, Y. R., *Nature* **1989,** *337* (6207), 519-525.

16. Raschke, M. B.; Shen, Y. R., *Curr. Opin. Solid St. M.* **2004,** *8* (5), 343-352.

17. Shen, Y. R., *Solid State Commun.* **1997,** *102* (2-3), 221-229.

18. Baldelli, S., *Acc. Chem. Res.* **2008,** *41* (3), 421-431.

19. Kataoka, S.; Cremer, P. S., *J. Am. Chem. Soc.* **2006,** *128* (16), 5516-5522.

20. Chen, X. Y.; Clarke, M. L.; Wang, J.; Chen, Z., *Int. J. Mod Phys B* **2005,** *19* (4), 691-713.

21. Azam, M. S.; Weeraman, C. N.; Gibbs-Davis, J. M., *J. Phys. Chem. C* **2013,** *117* (17), 8840-8850.

22. Salafsky, J. S., *PCCP* **2007,** *9* (42), 5704-5711.

23. Ok, K. M.; Chi, E. O.; Halasyamani, P. S., *Chem. Soc. Rev.* **2006,** *35* (8), 710-717.

24. Nagata, Y.; Mukamel, S., *J. Am. Chem. Soc.* **2010,** *132* (18), 6434-6442.

25. Nguyen, T. T.; Sly, C. L.; Conboy, J. C., *Anal. Chem.* **2012,** *84* (1), 201-208.

26. Conboy, J. C.; Kriech, M. A., *Anal. Chim. Acta* **2003,** *496* (1-2), 143-153.

27. Liu, Y.; Yan, C. Y.; Zhao, X. L.; Eisenthal, K. B., *Langmuir* **2001,** *17* (7), 2063-2066.

28. Malin, J. N.; Geiger, F. M., *J. Phys. Chem. A* **2010,** *114* (4), 1797-1805.

29. Liu, J.; Subir, M.; Nguyen, K.; Eisenthal, K. B., *J. Phys. Chem. B* **2008,** *112* (48), 15263-15266.

30. Harper, K. L.; Allen, H. C., *Langmuir* **2007,** *23* (17), 8925-8931.

31. Liu, J.; Conboy, J. C., *J. Am. Chem. Soc.* **2004,** *126* (27), 8376-8377.

32. Anglin, T. C.; Liu, J.; Conboy, J. C., *Biophys. J.* **2007,** *92* (1), L1-L3.

33. Chen, X. Y.; Chen, Z., *BBA-Biomembranes* **2006,** *1758* (9), 1257-1273.

34. Ouellette, R. J., *Organic Chemistry*. Second ed.; Prentice hall: upper saddle river, New jersey 07458, p 447.

35. Campbell, N. A., *Biology*. Seven ed.; Pearson: p 88-89.

36. Mahmoudian, L., The Central Dogma in Molecular Biology. In *Unravelling Single Cell Genomics: Micro and Nanotools*, Bontoux, N.; Dauphinot, L.; Potier, M. C., Eds. Royal soc chemistry: Cambridge, pp 15-25.

37. Donald Voet, J. G. V., *Biochemistry* Second ed.; John wiley & sons, Inc: p 830-831.

38. Yang, S.; Rothman, R. E., *Lancet Infect. Dis.* **2004,** *4* (6), 337-348.

39. Xing, Y. S.; Wang, P.; Zang, Y. C.; Ge, Y. Q.; Jin, Q. H.; Zhao, J. L.; Xu, X.; Zhao, G. Q.; Mao, H. J., *Analyst* **2013,** *138* (12), 3457-3462.

40. Kwok, J.; Kwong, K. M., *Brit. J. of Dermatol.* **2013,** *168* (3), 526-532.

41. Madico, G.; Quinn, T. C.; Rompalo, A.; McKee, K. T.; Gaydos, C. A., *J. Clin. Microbiol.* **1998,** *36* (11), 3205-3210.

42. de la Cruz, S.; Lopez-Calleja, I. M.; Alcocer, M.; Gonzalez, I.; Martin, R.; Garcia, T., *Food Control* **2013,** *33* (1), 105-113.

43. Studer, E.; Rhyner, C.; Luthy, J.; Hubner, P., *Z. Lebensm. Unters. F. A.* **1998,** *207* (3), 207-213.

44. Allmann, M.; Candrian, U.; Hofelein, C.; *Z. Lebensm. Unters. F. A.* **1993,** *196* (3), 248-251.

45. Surabattula, R.; Vejandla, M. P.; Mallepaddi, P. C.; Faulstich, K.; Polavarapu, R., *Exp. Parasitol.* **2013,** *134* (3).

46. Hu, J. A.; Zhang, C. Y., *Anal. Chem.* **2010,** *82* (21), 8991-8997.

47. Abdul-Ghani, R.; Al-Mekhlafi, A. M.; Karanis, P., *Acta Trop.* **2012,** *122* (3), 233-240.

48. Fu, L.; Tang, D.; Zhuang, J.; Lai, W.; Que, X.; Chen, G., *Biosens. Bioelectron.* **2013,** *47*.

49. Nuovo, G. J.; Margiotta, M.; MacConnell, P.; Becker, J., *Diagn. Mol. Pathol.* **1992,** *1* (2).

50. Gibellini, D.; Vitone, F.; Schiavone, P.; Ponti, C.; La Placa, M.; Re, M. C., *J. Clin. Virol.* **2004,** *29* (4), 282-289.

51. Nuriya, H.; Inoue, K.; Tanaka, T.; Hayashi, Y.; Hishima, T.; Funata, N.; Kaji, K.; Hayashi, S.; Kaneko, S.; Kohara, M., *J. Clin. Microbiol.* **2010,** *48* (11), 3843-3851.

52. Noordhoek, G. T.; Kolk, A. H. J.; Bjune, G.; Catty, D.; Dale, J. W.; Fine, P. E. M.; Godfreyfaussett, P.; Cho, S. N.; Shinnick, T.; Svenson, S. B.; Wilson, S.; Vanembden, J. D. A., *J. Clin. Microbiol.* **1994,** *32* (2), 277-284.

53. Moore, D. F.; Curry, J. I., *J. Clin.l Microbiol.* **1995,** *33* (10), 2686-2691.

54. Yamaguchi, A.; Nepote, J. A.; Kadivar, M.; Tagami, Y.; Fukushi, M.; Kikuchi, Y.; Sato, N.; Kikuchia, K., *Clin. Chim. Acta* **2002,** *316* (1-2), 147-154.

55. Van De Velde, H.; Sermon, K.; Lissens, W.; De Vos, A.; Van Steirteghem, A.; Liebaers, I., *J. of Assist. Reprod. Gen.* **1997,** *14* (8), 474-475.

56. Bansho, Y.; Ichihashi, N.; Kazuta, Y.; Matsuura, T.; Suzuki, H.; Yomo, T., *Chem. Biol.* **2012,** *19* (4), 478-487.

57. Walker, G. T.; Fraiser, M. S.; Schram, J. L.; Little, M. C.; Nadeau, J. G.; Malinowski, D. P., *Nucleic Acids Res.* **1992,** *20* (7), 1691-1696.

58. Walker, G. T.; Little, M. C.; Nadeau, J. G.; Shank, D. D., *P. Natl. Acad. Sci. USA.* **1992,** *89* (1), 392-396.

59. Fire, A.; Xu, S. Q., *P. Natl. Acad. Sci.USA.* **1995,** *92* (10), 4641-4645.

60. Kim, J.; Easley, C. J., *Bioanalysis* **2011,** *3* (2), 227-239.

61. Guatelli, J. C.; Whitfield, K. M.; Kwoh, D. Y.; Barringer, K. J.; Richman, D. D.; Gingeras, T. R., *P. Natl. Acad. Sci.USA.* **1990,** *87* (5), 1874-1878.

62. Versalovic, J.; Lupski, J. R., *Trends Microbiol.* **2002,** *10* (10), S15-S21.

63. Chang, C. C.; Chen, C. C.; Wei, S. C.; Lu, H. H.; Liang, Y. H.; Lin, C. W., *Sensors* **2012,** *12* (6), 8319-8337.

64. Mori, Y.; Nagamine, K.; Tomita, N.; Notomi, T., *Biochem. Bioph. Res. Co.* **2001,** *289* (1), 150-154.

65. Parida, M.; Sannarangaiah, S.; Dash, P. K.; Rao, P. V. L.; Morita, K., *Rev. Med. Virol.* **2008,** *18* (6), 407-421.

66. Ji, H. X.; Yan, F.; Lei, J. P.; Ju, H. X., *Anal. Chem.* **2012,** *84* (16), 7166-7171.

67. Zeng, Y.-P.; Hu, J.; Long, Y.; Zhang, C.-Y., *Anal. Chem.* **2013,** *85* (12).

68. Li, J. S.; Deng, T.; Chu, X.; Yang, R. H.; Jiang, J. H.; Shen, G. L.; Yu, R. Q., *Anal. Chem.* **2010,** *82* (7), 2811-2816.

69. Zhao, W. A.; Ali, M. M.; Brook, M. A.; Li, Y. F., *Angew.Chem. Int. Edit.* **2008,** *47* (34), 6330-6337.

70. Cheng, Y. Q.; Zhao, J. J.; Jia, H. L.; Yuan, Z.; Li, Z. P., *Analyst* **2013,** *138* (10), 2958-2963.

71. Ma, C. P.; Wang, W. S.; Yang, Q.; Shi, C.; Cao, L. J., *Biosens. Bioelectron.* **2011,** *26* (7), 3309-3312.

72. Coll, P.; Garrigo, M.; Moreno, C.; Marti, N., *Int. J. Tuberc. Lung D.* **2003,** *7* (9), 886-891.

73. *JAMA-J. Am. Med. Assoc.* **2000,** *284* (7).

Chapter 2

Real-time Monitoring of Phospholipase Catalyzed Reactions on Symmetric Lipid Bilayers Using Nonlinear Optical Spectroscopy

The SFG spectroscopy work from this chapter was done with the help of Dr. Champika Weeraman.

2.1 Chapter Overview

Phospholipases are a family of interfacial enzymes that catalyze the hydrolysis of cellular L-phospholipid molecules. It is believed that they play an important role in a variety of biochemical processes such as lipid metabolism and cellular signal transduction. In addition to these functions, phospholipases are most likely involved in the development of certain diseases, such as promoting breast tumor growth, and play a role in the inflammatory response.[1,2] This chapter describes a real-time, in situ way to monitor the hydrolysis reaction catalyzed by phospholipase D (PLD) and phospholipase C (PLC) on a planar supported symmetric lipid bilayer. Owing to the asymmetry requirements of SFG, the hydrolysis reaction can be monitored by tracking the changes in SFG signal from the lipid head groups in the C-H vibrational region. In addition, a complementary SHG study is introduced based on enzyme-induced changes in the surface potential of the lipid bilayers. Unlike previous nonlinear optical studies, these investigations are the first example of directly monitoring the lipid structure at symmetric bilayers. Consequently, this work opens the door to future studies using lipids extracted from cells rather than labeled lipids typically employed in nonlinear optical spectroscopy experiments on planar lipid bilayers.

2.2 Introduction

A membrane-bound enzyme phospholipase D (PLD) is a ubiquitous enzyme that catalyzes the cleavage of phosphatidylcholine (PC) to yield phosphatidic acid (PA) and release a choline. The activation of the PLD in cells usually results in a

several fold increase in PA, which is a bioactive lipid.[3] Specifically, the signaling molecule lipid PA serves as a second messenger, which is involved in different signal transductions, such as neurotransmitters and growth factors associated with intercellular communication.[4,5,6] For example, PA can be further metabolized to bioactive diacylglycerol or lyso-PA (LPA), which affects many significant cellular processes, including cell proliferation, migration and survival.[7,8]

Phospholipase C (PLC) catalyzes PC hydrolysis to yield diacylglycerols (DAG) and release a phosphocholine. There are some studies that indicate that PLC and PLD are potential tumor promoters and their hydrolytic products, particular DAG and PA, are likely to be involved in promoting tumor growth.[2, 9]

In order to improve the understanding of these enzymes and involved mechanisms of the enzyme-induced hydrolysis processes, phospholipase activity has been studied by several established methods including fluorescent assays[10], radioactive assays[11], choline monitoring with a choline oxidase-oxygen electrode[12], atomic force microscopy (AFM)[13,14] and polarization modulation infrared reflection-absorption spectroscopy on lipid monolayers at the air-water interface (PM-IRAS).[15,16,17] However, the mechanism of this hydrolysis process is not fully understand on the planar support. For example, depending on the hydrolysis product of the lipid, the order of the hydrolysis of the two leaflets may be different. Therefore a spectroscopic method that allows for the direct *in situ* measurement of the conformation and symmetry changes of the lipid bilayer is important.

Vibrational sum frequency generation spectroscopy is widely used to study in real-time the interfacial structures, dynamics and orientations of lipids[18] and other biomolecules (such as peptides and proteins) in model membrane systems.[21,22,23] This technique has several advantages over the others, including surface specificity, and the ability to monitor reactions *in situ*, in real time without the use of labels.[16,24] Recently, VSFG has also been employed to monitor phospholipase A_2 catalysis at asymmetric membranes.[26]

One important aspect of the behavior of lipids in cell membranes is their ability to translocate both laterally and across the membrane (flip-flop). As SFG requires a break in inversion symmetry VSFG have been employed to measure this process based on the degree of asymmetry or population inversion in lipid membranes using asymmetric bilayers composed of a deuterated leaflet and a protonated leaflet. With these asymmetric bilayers, the Conboy group[20] and several other groups[25] demonstrated that SFG is amenable to monitoring lipid translocation (flip-flop) kinetics with minimal labeling, which allows for the direct study of membrane lipid dynamics using only native lipid species without the need for exogenous fluorescent or spin-labeled probes. Significantly, Conboy and co-workers revealed that the chemical modification of lipid species with a fluorescent or spin-labeled probe can significantly alter the intrinsic rate of lipid translocation (flip-flop).[26]

More recently, Ye and co-worker studied the hydrolysis process of phospholipase A_2 (PLA_2) on a supported asymmetric phospholipid bilayer.[27] Using SFG, they investigated the structural change and symmetry of lipid bilayers

using the terminal CH_3 group from the acyl chain as an indicator. Using a hydrogenated lipid L-DPPC and the deuterated enantiomer D-DPPC-d_{75} resulted in the asymmetric L-DPPC (distal)/ D-DPPC-d_{75} (proximal) bilayer. By monitoring the C-H stretching and C-D stretching modes of the methyl and methylene groups from the acyl chain of the lipids, they observed that the hydrolysis process of the asymmetric bilayer started from the distal leaflet, which then underwent a movement that exchanged the position between distal and proximal lipids, resulting in the two leaflets being hydrolyzed simultaneously.[27]

Although VSFG has led to a greater understanding of lipid dynamics and other processes involving interactions at bilayers the requirement of an asymmetric bilayer has limited VSFG investigations to model membrane systems.[16, 24] Herein, we describe using VSFG and the complementary nonlinear optical technique second harmonic generation (SHG) to monitor the cleavage of phosphatidylcholine (PC) by phospholipase D in symmetric lipid bilayers. Although a deuterated lipid is employed throughout the VSFG investigation to isolate the vibrational signatures of the PC head group, these experiments establish that VSFG can be used to monitor the structural changes of lipids on symmetric bilayers. This work is a critical first step in the ultimate goal of using VSFG to probe lipids extracted from cells as well as the direct investigation of cellular membranes. Moreover, the ability to use the complementary and simpler technique SHG to monitor reactions of the lipid is also promising as SHG is widely employed in microscopy as well as spectroscopic investigations.

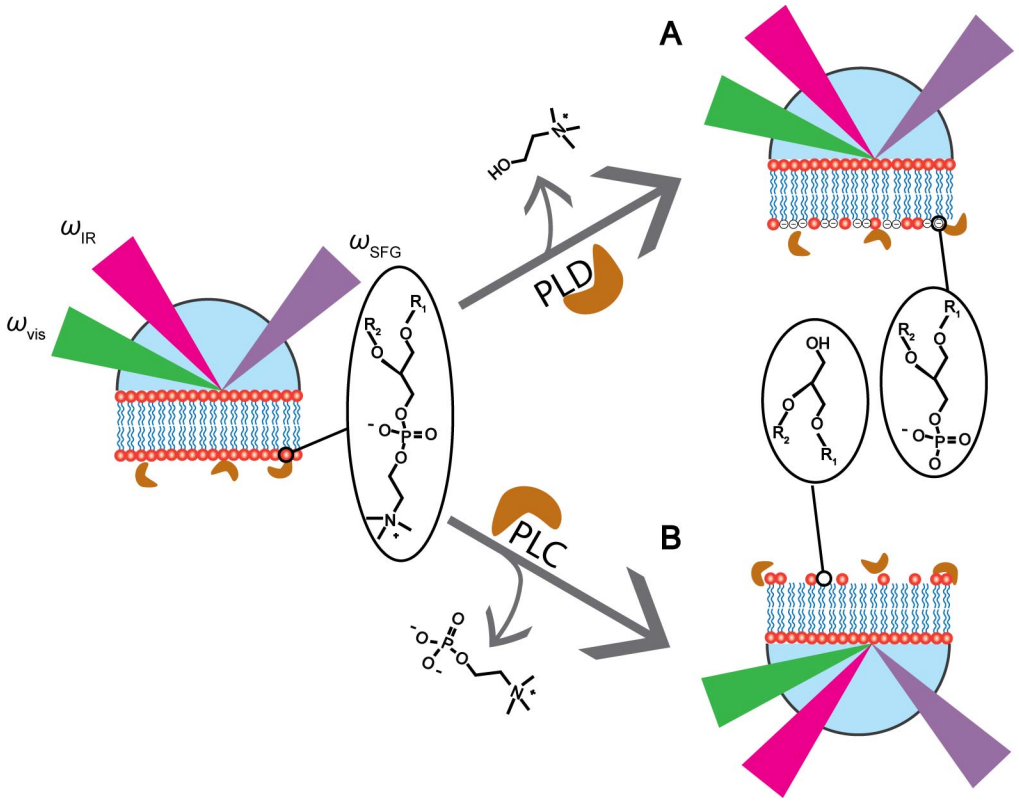

Figure 2.1 A schematic representation of monitoring the hydrolysis reaction of PLD and PLC on a planar lipid bilayer. (A) As PLD is introduced, the choline is released leaving a negatively charged phosphatidic acid (PA) on the surface. (B) As the PLC is introduced to the cell, a phosphate choline is released leaving a neutral-charged lipid (DAG) on the surface. R_1, R_2 = fatty acids

2.3 Experimental

2.3.1 Materials

Deuterium oxide (D_2O, 99.9%) was purchased from Sigma-Aldrich. GC grade chloroform (CH_3Cl), methanol (CH_3OH) and calcium chloride hexahydrate were supplied from Caledon Laboratories. Tris base was purchased from Fisher Chemicals. 1-palmitoyl-2-oleoyl-*sn*-glycero-3-phosphocholine (POPC) and 1,2-dipalmitoyl-*sn*-glycero-3-phosphocholine (DPPC-d_{62}) were obtained from Avanti Polar Lipids as either a lyophilized power or dissolved in CH_3Cl. All the lipids

were stored in the freezer (-20°C) and used without any further purification. Structures of the lipids used are found in Figure 2.2. Phospholipase D (PLD) from *Streptomyces chromofuscus* and Phospholipase C (PLC) from *Bacillus cereus* were purchased from EMD Millipore and stored in the freezer (-20°C). The water used in these studies was purified by a Milli-Q-Plus ultrapure water purification system (Millipore) leading to a maximum resistivity of 18.2 MΩ.cm. An IR and UV grade fused silica hemisphere (ISP optics, 1 in. diameter, QU-HS-25, UV grade SiO_2) were used for the planar supported lipid bilayers ($PSLB_S$) in the SFG and SHG experiments, respectively. The hemispheres were immersed in a piranha solution of concentrated sulfuric (from Caledon Laboratories) acid and 30%-hydrogen peroxide (from Sigma-Aldrich) with the ratio 3 to 1 to remove any organics on the surface prior to introducing the lipid bilayer.

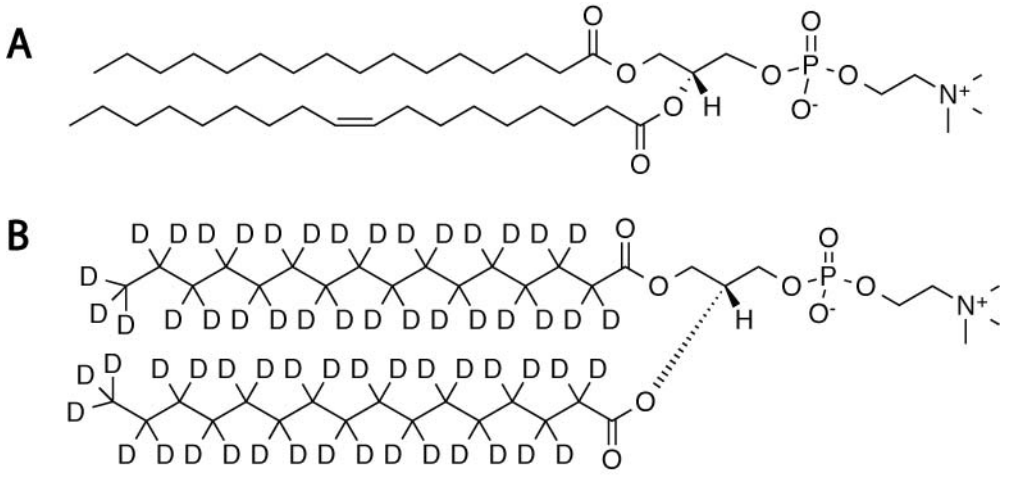

Figure 2.2 Chemical structure of phospholipids used in the study: (A) POPC and (B) DPPC-d_{62}.

2.3.2 Preparation of planar supported lipid bilayers

The UV or IR grade fused silica hemisphere was cleaned prior to use by sonicating it in Millipore water followed by methanol and then water, dried in the oven and then cleaned by submerging into a piranha solution of 70% sulfuric acid (18M)/ 30% hydrogen peroxide (30%) for at least 1 hour at 100 ºC. The hemisphere was then rinsed thoroughly with copious amount of Millipore water followed by sonicating in water (5 minutes × 2), in methanol (5 minutes), and in water (5 minutes) as a final step. Then the hemisphere was allowed to dry in an oven at 100 ºC for about 10 minutes, cooled down to room temperature and then plasma cleaned (plasma cleaner, PDC-32G, Harrick Plasma) in air for 2 minutes just prior to use.

Planar lipid bilayers (PLBs) supported on a fused silica hemisphere used in this study were prepared by vesicle fusion from a 1-palmitoyl-2-oleoyl-*sn*-glycero-3-phosphocholine (POPC) or 1,2-dipalmitoyl-*sn*-glycero-3-phosphocholine (DPPC-d_{62}) vesicle suspension. Briefly, appropriate amounts of lipids dissolved in chloroform were mixed in a glass vial to obtain a final concentration of 1 mg/mL. The chloroform was then evaporated by consistently blowing a gentle stream of nitrogen for three hours to get a thin uniform lipid film. This film was then placed into a desiccator under vacuum for two hours. Next, the lipid film was reconstituted in buffer (10 mM $CaCl_2$, 50 mM Tris-HCl buffer, pH 8) to reach a final lipid concentration of 1 mg/mL. The lipids were suspended in solution by vortexing for two minutes at low speed. The vesicles were then formed by placing the lipid suspension in a sonicator for 30 minutes at

room temperature for POPC or around 45°C for DPPC-d_{62} until the suspension was clear. The lipid bilayers were formed on the fused silica hemispheres by immersing them in the vesicle solution for about 30 minutes at room temperature for POPC and one hour around 45°C for DPPC-d_{62}. The hemispheres were carefully transferred to a Petri dish containing Tris buffer (10 mM $CaCl_2$, 50 mM Tris, pH 8) to remove the excess vesicles. The hemispheres were assembled in our custom-made flow cell submerged in a Petri dish under buffer bath to avoid exposing the flat surface to the air. After assembling the flow cell and placing it on the flow set-up on the laser table, depending on the buffer used in the enzyme study, a Tris or bicarbonate buffer mixture in D_2O (10 mM $CaCl_2$, 50 mM Tris, pH 8 or 120 mM NaCl, 4 mM KCl, 1.5 mM $CaCl_2$, 1.0 mM $MgCl_2 \cdot 6H_2O$, 25mM $NaHCO_3$, pH 7.3) was flowed by the sample at a rate of 5 ml/hr for one hour prior to introducing the enzyme for all the SFG experiments.

2.3.3 Ultrafast laser assembly

A femtosecond Ti:Sapphire oscillator (Spectra Physics, Maitai, 80 MHz, 1.0 W) was used to produce pulses centered at 800 nm (<100fs, FWHM ~12 nm). This pulse was used as the seed pulse in a regenerative amplifier (Spitfire Pro, Spectra Physics, 1 kHz, 100 fs, 3.3 W) pumped by a Nd:YLF laser (Spectra Physics, Empower, 11.5 W), which resulted in fs-pulses with high peak power (1 kHz, 3.3 mJ per pulse).

2.3.3.1 Sum frequency vibrational spectroscopy set-up

Broadband sum frequency generation experiments that were performed in this study used two-thirds of the Spitfire Pro output regeneratively amplified system described above (2.2 W) to pump a TOPAS-C/NDFG optical parametric amplifier (Light Conversion) (Figure2.1). The resulting broad bandwidth infrared beam (FWHM ~ 150 cm^{-1}) is tuned from 2700 to 3000 cm^{-1} to probe the resonance of the C-H stretching region of the silica/water interface. Visible light from the spitfire (100 fs, λ= 800nm) was broadend to a picosecond pulse using a Fabry-Perot etalon (FWHM ~ 10 cm^{-1}). P-polarized femtosecond IR light (~10-12 μJ/pulse) and s- or p-polarized picosecond visible light (~10 μJ/pulse) were then temporally and spatially overlapped onto the flat surface of a fused silica hemisphere mounted onto our custom-built Teflon flow cell at incident angles of 66° and 64°, respectively, from the surface normal (Figure 2.3). After spatially and temporally overlapping at the sample surface, the reflected sum frequency beam from the sample was recollimated, optically filtered by a bandpass filter to remove residual 800 nm light (Chroma, HQ 617/70 M), passed through a polarizer to select s-polarized or p-polarized SFG, focused onto a spectrograph (Acton SP-2556 imaging spectrograph, grating: 1800 grooves/mm with 500 nm blaze wavelength) and then detected by a charge-coupled device camera (Acton PIXIS 100B CCD digital camera system, thermoelectrically cooled, back-illuminated, 1340×100 pixels, 20μm×20μm pixel size, Princeton Instruments). Before performing an experiment, a reference spectrum was first collected using the same configuration with a gold-coated silica hemisphere with the IR centered

around 2900 cm^{-1}. Spectra were then collected at the buffer/supported bilayer interface with the IR centered at the same wavelength. The spectra were normalized by dividing the measured spectra by the gold reference spectrum collected on the same day.

The SFG spectrum is polarization-dependent. In this study ssp (s-polarized sum-frequency, s-polarized visible, and p-polarized IR) and ppp (p-polarized SFG signal, p-polarized visible, and p-polarized IR) polarization combinations of the input and signal beams were used.

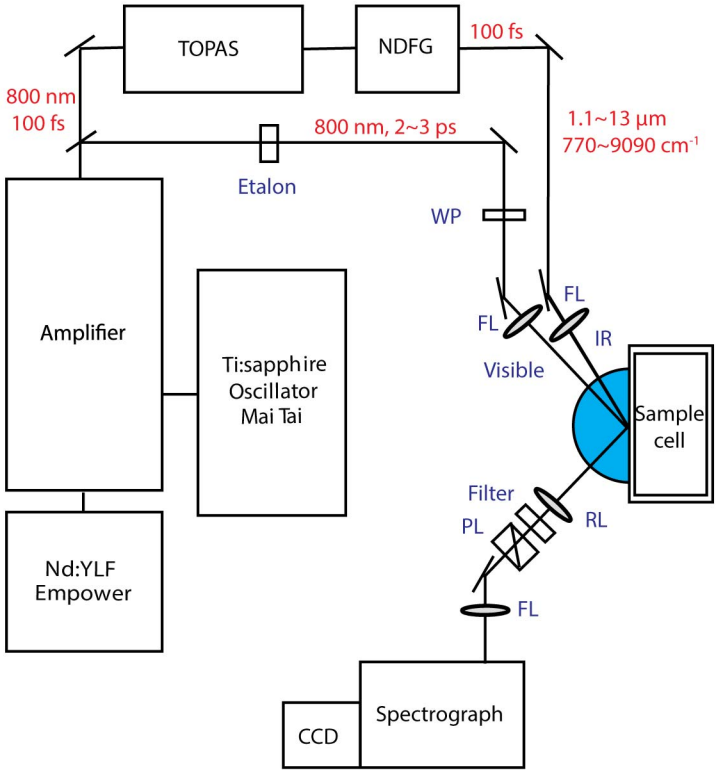

Figure 2.3 A schematic representation of the SFG set up. WP = half wave-plate; PL = polarizer; FL= focusing lens; RL = recollimating lens.

2.3.3.2 Second harmonic generation set-up

The Spitfire output was passed through a beam splitter and the transmitted output (1.1 W), which is one-third of the Spitfire output, was used to pump an optical parametric amplifier (Spectra Physics OPA-800CF) (Figure 2.4). The output from the OPA (tuned to 550 ± 2 or 590 ± 2 nm) was attenuated to 0.4 ± 0.1 μJ by a neutral-density filter (New Focus, cat. # 5215) and directed through a half-wave plate and polarizer for p-polarization selection. The polarized light was focused onto the supported lipid bilayer/buffer interface at an angle of 62° from the surface normal near total internal reflection. The reflected second harmonic light generated at the interface then passed through a color glass filter (Thorlabs) to remove the reflected fundamental light and was focused onto a monochrometer (Optometrics Corp., MiniChrom MC1-02) tuned to the second harmonic wavelength (275 nm or 295 nm) (Figure 2.4). SHG was detected by gated photon counting using a photomultiplier tube (PMT, Hamamatsu Photonics) connected to a pre-amplifier and a photon counter (Stanford Research Systems). Before performing each experiment, the quadratic power dependence and SHG wavelength dependence were verified to ensure no optical damage was occurring at the interface.

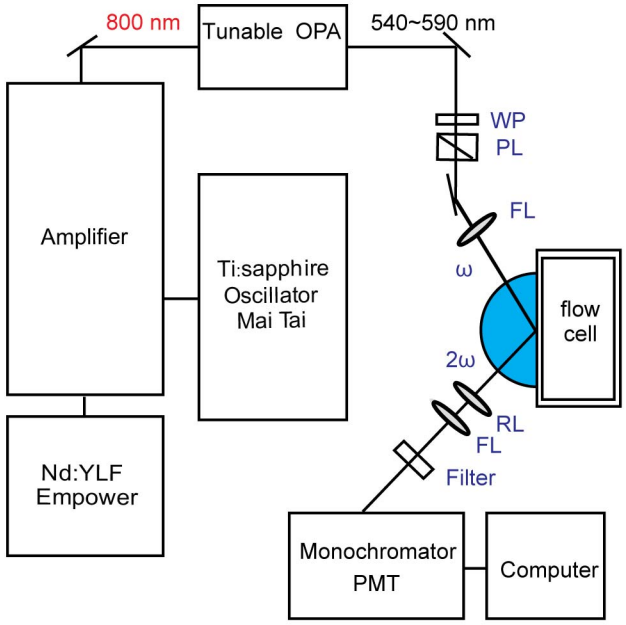

Figure 2.4 A schematic representation of the SHG set up. WP = half wave-plate; PL = polarizer; FL= focusing lens; RL = recollimating lens.

2.3.4 DPPC-d_{62} and DOPC bilayers hydrolysis reaction with PLD and PLC

The enzymatic hydrolysis of DPPC-d_{62} and DOPC were monitored as a function of enzyme and lipid structures using SFG and SHG in real-time at room temperature. For the PLD experiments, 20 units PLD/ 1.5 ml added at the rate of 2 ml/hr were used with the optimized buffer for PC hydrolysis by PLD (50 mM Tris, 10mM $CaCl_2$, pH 8).[25] The PLC induced hydrolysis reactions were studied with the same flow rate, the same buffer and two different enzyme concentrations (1.5 units/1.5 ml and 20 units/1.5ml). The optimized buffer for the reaction with PLC was also used (120 mM NaCl, 4 mM KCl, 1.5 mM $CaCl_2$, 1.0 mM $MgCl_2 \cdot 6H_2O$, 25 mM $NaHCO_3$, pH 7.3). Control experiments were also

performed using bovine serum albumin at a higher concentration in the same manner, by flushing the cell with Tris buffer in D_2O, followed by Tris buffer in D_2O containing 10 mg/mL BSA.

2.4 Results and Discussion

2.4.1 Sum frequency vibrational spectroscopy at the planar supported bilayer interfaces

Planar supported lipid bilayers (PLBs) have been widely used as a biological model to mimic many aspects of cell membrane behavior.[29,30,31,32] SFG has been utilized to study bilayer behavior due to its surface specificity, and ability to monitor reactions in real time with structurally minimal labeling. In the past several years, SFG has proven to be a powerful tool for studying the interfacial structure of lipids, proteins and peptides.[23,32] In particular, the Conboy group has measured the phase transition temperature and transbilayer movement (flip-flop or translocation) of asymmetric planar supported phospholipid bilayers based on the SFG-active symmetric C–H stretching modes of the methyl groups terminating the hydrophobic lipid chains.[22,25,34] By focusing on spectral signatures associated with amino acids, the Chen group has studied the adsorption kinetics of protein and peptides with lipid bilayers.[35] In one example, they monitored the peptide metlittin interacting with symmetric bilayers (POPG/POPG) based on the spectral signatures of the peptide. SFG signal changes were also observed from the terminal methyl from the lipid acyl chain, which indicated that the peptide affected the lipid order.[35,36] With respect to the study of enzyme-catalyzed

reactions at bilayer interfaces, the Ye group successfully monitored the hydrolysis of DPPC by phospholipase A_2 (PLA_2) in an asymmetric planar supported phospholipid bilayer indirectly by observing the spectroscopic changes in the methyl groups terminating the hydrophobic chains.[27]

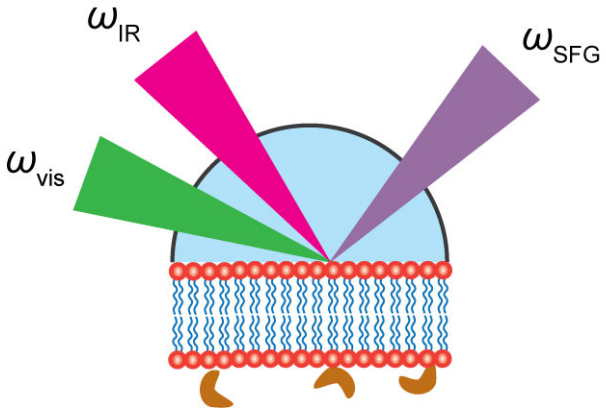

Figure 2.5 Schematic of SFG monitoring of the phospholipase-induced hydrolysis reaction at a symmetric phospholipid bilayer supported on a silica hemisphere.

The recent work of Ye established that SFG was suitable for monitoring enzymatic reactions at supported bilayer interfaces.[27] However, this previous work depended on the use of an asymmetric bilayer consisting of a deuterated leaflet and a protonated leaflet. As a result of the many C-H groups present on the protonated lipid tail, the PC head group was not readily observed by SFG. Fortunately, the reaction of phospholipase A_2 (PLA_2) with the bilayer led to a significant decrease in the signal originating from the deuterated and protonated lipid tails, which the authors attributed to desorption of the bilayer after the hydrolysis reaction. One disadvantage of this approach is its requirement of asymmetric bilayers, containing a deuterated leaflet and protonated leaflet, which

are more difficult to form and limit the type of lipids that can be explored by SFG. Thus, our aim is to monitor enzymatic reactions on symmetric lipid bilayers using the polar head group as an indicator to probe the whole hydrolysis process.

In these experiments, we employed a symmetric planar lipid bilayer, DPPC-d_{62}/DPPC-d_{62}, supported on IR-grade fused silica and monitored the structural changes based on the SFG signature of the phosphatidyl choline head group, which was protonated in contrast to the lipid tails that were deuterated (Figure 2.2). Here, we successfully demonstrate the use of SFG to detect PLD and PLC catalyzed hydrolysis reactions on planar supported symmetric lipid bilayers by tracking the SFG signal changes of the head group *in situ*. Not only does this represent the first investigation of enzymatic reactions at symmetric lipid bilayers using SFG, it is also the first observation of PLC hydrolysis on planar supported phospholipid bilayers.

2.4.1.1 Monitoring the phospholipase D catalyzed reaction at the DPPC/buffer interface

A FTIR spectrum of DPPC-d_{62} was obtained as a reference for all the SFG experiments (Figure 2.6). The spectral region between 2800-3100 cm^{-1} (C-H stretching region) was monitored to obtain the spectral features of the perprotonated head group. Three strong peaks were found in the FTIR spectrum at 2962 cm^{-1}, 2952 cm^{-1} and 2923 cm^{-1}, the assignments of which will be discussed later. Similarly, vibrational SFG spectra were obtained at the DPPC-d_{62}/buffer interface (in D_2O) also in the C-H stretching region (2800-3000 cm^{-1}) (Figure

2.7). Two polarization combinations were used to aid in resolving symmetric and asymmetric vibrational modes: p-polarized SFG, p-polarized visible and p-polarized IR (ppp) and s-polarized SFG, s-polarized visible and p-polarized IR (ssp) (Figure 2.7A-B and C-D, respectively). As the bilayer consisted of assembling a single type of lipid, we expected nearly complete cancellation of the SF signal arising from the C-H stretches in the PC head groups due to the centrosymmetry of the lipid bilayer on the planar surface. Representative ppp and ssp VSFG spectra of a symmetric DPPC-d_{62}/DPPC-d_{62} bilayer are shown in Figure 2.8 (green trace). Indeed, there was very weak SFG signal from this neutral, zwitterionic lipid bilayer owing to near cancellation of the C-H oscillators on opposite leaflets. The most prominent peak for both the ppp (left) and ssp (right) spectra was centered at 2985 cm^{-1}, and a weak shoulder around 2925 cm^{-1} was also observed (Figure 2.8).

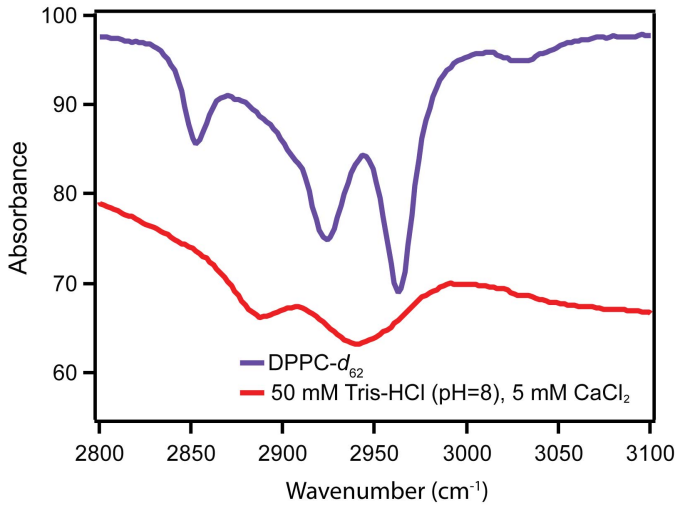

Figure 2.6 The FTIR spectrum of DPPC-d_{62} (purple) and Tris buffer (5 mM $CaCl_2$, 50 mM Tris, pH 8).

As displayed in Figure 2.7A and 2.7B, upon adding PLD the signal originating from the PC head groups increased significantly in the ppp spectra of the DPPC-d_{62}/DPPC-d_{62} bilayer. At 55 minutes, the SFG intensity reached a maximum, with peaks appearing at 2910 cm^{-1} and 2967 cm^{-1}. The SFG signal dropped dramatically around 61 minutes and mostly vanished by 71 minutes (Figure 2.8, left panel).

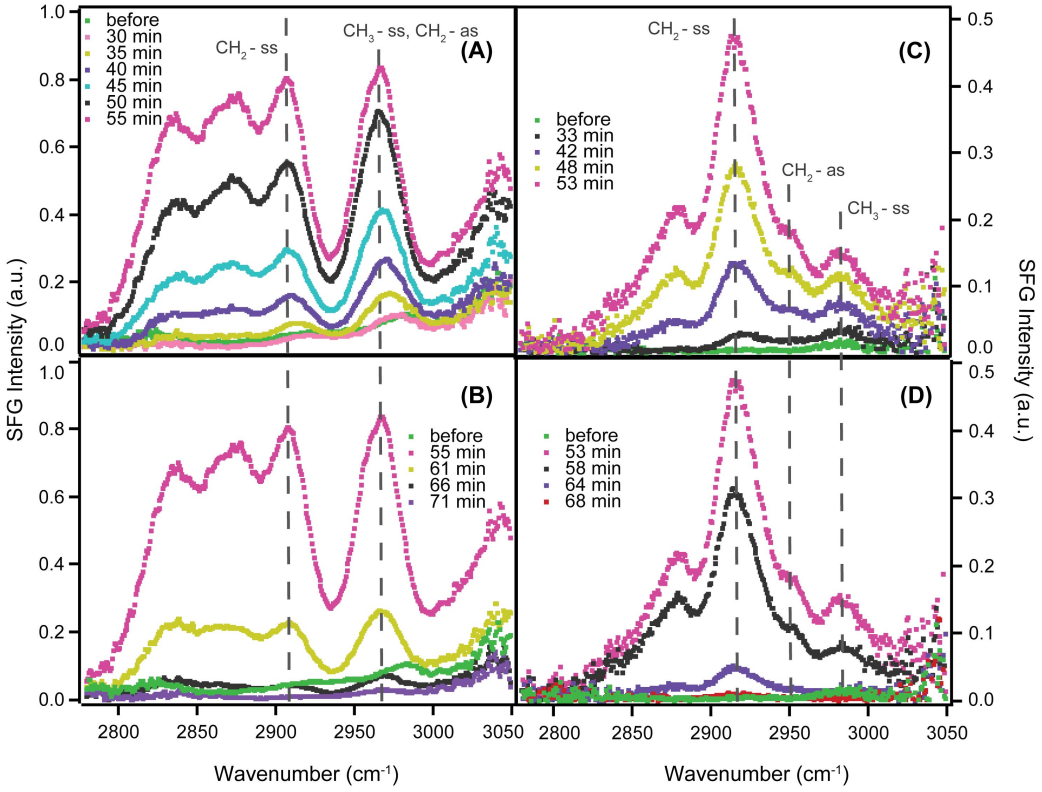

Figure 2.7 The C-H stretching frequency region collected from a DPPC-d_{62}/DPPC-d_{62} bilayer. SFG ppp spectra taken (A) from 0 to 55 min; (B) from 55 to 71 min. SFG ssp spectra taken (C) from 0 to 53min; (D) from 53 to 68 min (D). The experiment was conducted in Tris-buffer (pH=8) with 20 units/1.5mL PLD in real-time at room temperature.

Based on studies from the Conboy and Allen groups[18,19,20], we assign the frequency at 2967 cm^{-1} to a combination peak, which originates from the methyl

symmetric stretch (CH_3-ss) and the methylene asymmetric stretch (CH_2-as) from tetraalkyl ammonium group of the phosphocholine. The frequency at 2910 cm^{-1} is assigned to the CH_2-ss from the same methylene group in phosphocholine. There are additional peaks in the ppp spectrum after 55 minutes of the reaction at 2838 and 2878 cm^{-1}. They are likely to be CH_2-ss from the methylene groups neighboring the ester and phosphate groups, respectively.

The same trend of increasing SFG signal was also observed in the ssp spectra (Figure 2.7 C and D); the peak at frequency 2983 cm^{-1} is assigned to the CH_3-ss from the phosphocholine head group and at 2951 cm^{-1} is assigned to the CH_2-as from the CH_2 adjacent to the nitrogen. The peak observed at 2915 cm^{-1} can be assigned to the corresponding CH_2-ss. Once again, after 73 minute all peaks had disappeared as shown in Figure 2.8 (right panel, black trace). There are two explanations for the peak disappearance, which I will state in later text.

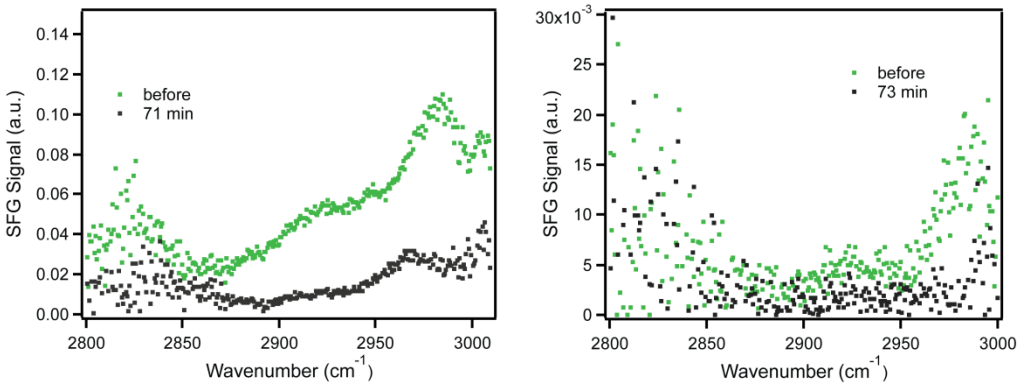

Figure 2.8 SFG ppp (left) and ssp (right) spectra of the C-H stretching region collected from a DPPC-d_{62}/DPPC-d_{62} bilayer before (green) and after (black) the reaction with PLD. The data in the spectra are rescaled from Figure 2.7 to observe the difference in SFG intensity before and after reaction. This indicates changes in the lipid layer composition before and after reaction.

Figure 2.9 exhibits the SFG intensity changes from the CH_2 and CH_3 of the ammonium group with time. A very weak SFG signal was observed before introducing the PLD, and the signal increased as the hydrolysis reaction proceeded. After reaching its maximum around 50 minutes, it decayed almost to zero over ~ 20 minutes. We propose that the PLD first catalyzed the cleavage of the DPPC group resulting in a DPPA in the top leaflet and the release of free choline (Figure 2.1). The result was an asymmetric bilayer with DPPC in the bottom leaflet and a mixture of DPPA and DPPC in the top leaflet. Consequently, the signal associated with the polar head groups increased because of the increase in their net orientation (the lack of cancellation). The signal decrease, however, could result from two possibilities: flip-flopping of the lipids after hydrolysis and complete desorption of the lipid bilayer from the silica surface. As previously mentioned, lipids have been found to exchange position or flip flop between leaflets.[20, 23] During the reaction, a small amount of DPPA could have flipped to the bottom leaflet. As the DPPA flipped to the bottom leaflet, it was then replaced by a DPPC molecule. The reaction continued with hydrolysis of the lower DPPC that flipped to the top until all DPPC was exhausted. With the loss of the choline group, the resulting DPPA/DPPA bilayer would not contain any vibrational modes above 2900 cm^{-1}. The second explanation for the sudden decrease in signal is the accumulation of negatively charged DPPA molecules that destabilize the bilayer and promote desorption from the negatively charged surface due to the repulsion. This could also explain why the SFG signal was lower than the initial signal, as a consequence of having little to no lipid on the surface. Finally, a

combination of both processes is likely. Specifically, the DPPA as it formed could have exchanged position in the bilayer leading to a decrease in signal until a critical concentration was reached and the membrane desorbed from the surface. This would explain the gradual SFG signal decrease until it eventually vanished.

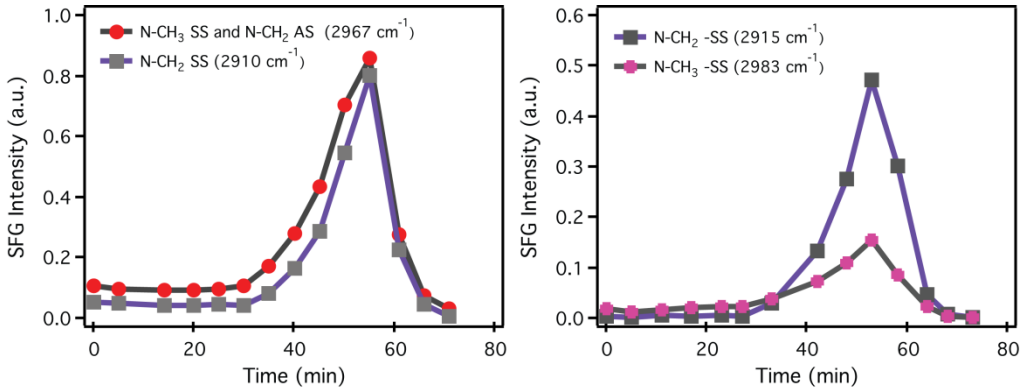

Figure 2.9 SFG intensity changes for CH_3-ss and CH_2-ss at different times from ppp (left) and ssp (right) spectra.

2.4.1.2 Monitoring the Phospholipase C Catalyzed Reaction at the DPPC/Buffer Interface

To verify that this VSFG method for monitoring reactions at lipid bilayers was general, a similar experiment was conducted with phospholipase C (PLC). Unlike PLD which generates a negatively charged phosphatidic acid from the zwitterionic phosphocholine head group, hydrolysis by PLC results in a neutral diacyglycerol and loss of phosphocholine (Figure 2.1). Figure 2.10 exhibits the time-dependent change of the ppp and ssp SFG signal in the C-H stretching region (2850-3050 cm^{-1}) with 20 units/1.5mL PLC in Tris-buffer (in D_2O).

As had been previously observed, the starting SFG signal was very weak due to the centrosymmetry of the DPPC-d_{62}/DPPC-d_{62} bilayer. After adding the

enzyme, the ppp spectra exhibited increases at 2911 cm^{-1} and 2972 cm^{-1}, which were assigned to the CH_2-ss and CH_3-ss of the phosphocholine head group, respectively, as described in the PLD experiments. In addition, one weak resonance at 2880-2885 cm^{-1} appeared as the reaction proceeded, which was also present in the PLD experiments and assigned to the CH_2-ss for the methylene groups in the glycerol backbone or those neighboring the phosphate group. For the reaction with PLC, the SFG ssp spectra exhibited an increase in the peak centered at 2917 cm^{-1} (CH_2-ss; -CH_2-$N^+(CH_3)_3$) with time. The peak at 2985 cm^{-1} (CH_3-ss; -CH_2-$N^+(CH_3)_3$) remained the same intensity.

These PLC experiments yielded a similar trend where the SFG signal intensity of the head group increased as the reaction proceeded, which supports that the reaction occurred primarily on one leaflet leading to a break in the centrosymmetry of the phospholipid bilayer. However, unlike the PLD experiments, the signal did not drop after increasing. We propose that the DAG product is not as destabilizing to the lipid bilayer as the DPPA product from PLD. Consequently the lipid bilayer does not desorb from the surface. Additionally, the PLC experiments also only resulted in modest increases in SFG intensity. As shown in Figure 2.10, the changes in SFG intensities of the lipid bilayer after the PLC-catalyzed hydrolysis reaction were much lower than that of the PLD experiments. The hydrolysis product DPPA/DPPC from PLD might have an indirect influence on the VSFG spectra measurement. As the DPPA is negatively charged, it should increase the interfacial potential at the bilayer interface,

resulting in the enhancement of the $\chi^{(3)}$ term that can also contribute to SFG. Therefore, a more enhanced SFG intensity is expected.[37]

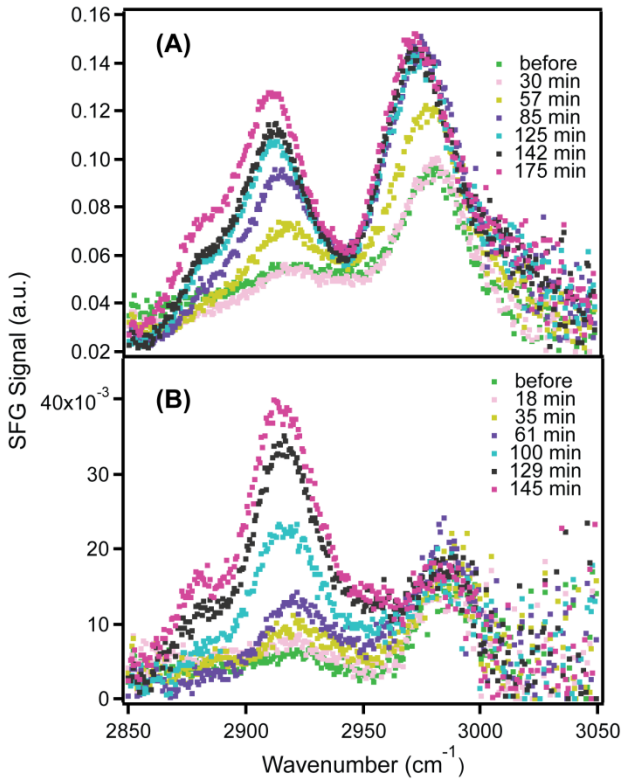

Figure 2.10 SFG ppp (A) and ssp (B) spectra of the C-H stretching frequency region collected from a DPPC-d_{62}/DPPC-d_{62} bilayer in Tris-buffer (pH 8) with 20 units/1.5mL PLC in real-time at room temperature.

The PLC experiment was performed in Tris buffer at pH 8 for a direct comparison with the PLD experiment. However, the optimal buffer for PLC is a bicarbonate buffer at pH 7.3. Figure 2.11 shows the PLC induced hydrolysis reaction with time profile using this optimized bicarbonate buffer (120 mM NaCl, 4 mM KCl, 1.5 mM $CaCl_2$, 1.0 mM $MgCl_2 \cdot 6H_2O$, 25 mM $NaHCO_3$, pH 7.3). Unlike both the PLC and PLD experiments performed in Tris-buffer where the

signal initially increased, in the experiments performed in bicarbonate buffer the signal immediately decreased upon adding the enzyme. With the higher concentration of PLC (20 units/1.5mL), the SFG signal intensity decreased rapidly and had almost disappeared after 90 minutes (Figure 2.11A-B). One possible origin of this initial decrease in signal was that the PLC induced hydrolysis reaction and lipid flip flop occurred rapidly leading to the formation of a more ordered bilayer with inversion symmetry and a corresponding drop in SFG signal (Figure 2.11A-B). Another possibility is that the PLC reacted simultaneously with both leaflets under these experimental conditions. The final possible explanation is that the hydrolysis product DAG immediately disordered the bilayer or led to its desorption from the surface. In contrast, when a very low concentration (1.5 unit/1.5mL) of PLC was injected, the SFG signal intensity initially decreased a little, followed by an increase with time (Figure 2.11C-D) as was observed in the experiments in Tris-buffer. We reason that DAG formed primarily on one leaflet, which could locally break the inversion symmetry even with lipid flipping. Alternatively, the small amount of DAG formed was stable and able to maintain the bilayer on the surface.

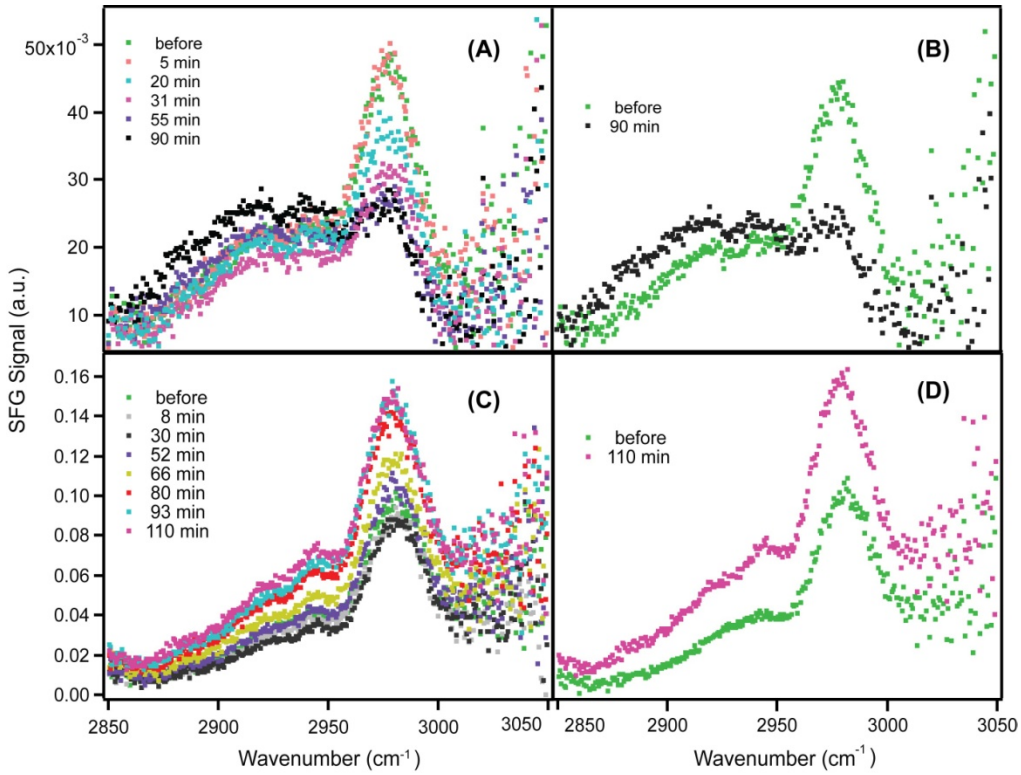

Figure 2.11 SFG ppp spectra of the C-H strethching frequency region collected from a DPPC-d_{62}/DPPC-d_{62} bilayer in bicarbonate buffer (pH 7.3) with 20 units/1.5 mL PLC (A) and 1.5 unit/1.5 mL PLC (C). The (B) and (D) are the spectra extract from before the injection of PLC and after.

2.4.1.3 Control experiment without the addition of enzyme

To verify that the Tris-buffer, which contained methylene groups, was not contributing to the signal over time, we monitored the SFG while flowing the buffer passed the sample. Specifically, SFG was monitored from a DPPC-d_{62}/DPPC-d_{62} bilayer in Tris-buffer solution without adding PLD or PLC (Figure 2.12). Both the ppp and ssp spectra indicated that the SFG signal changes were very small with time compared with the enzyme induced hydrolysis reaction. Therefore, we conclude that Tris-buffer has a negligible impact on the signal changes.

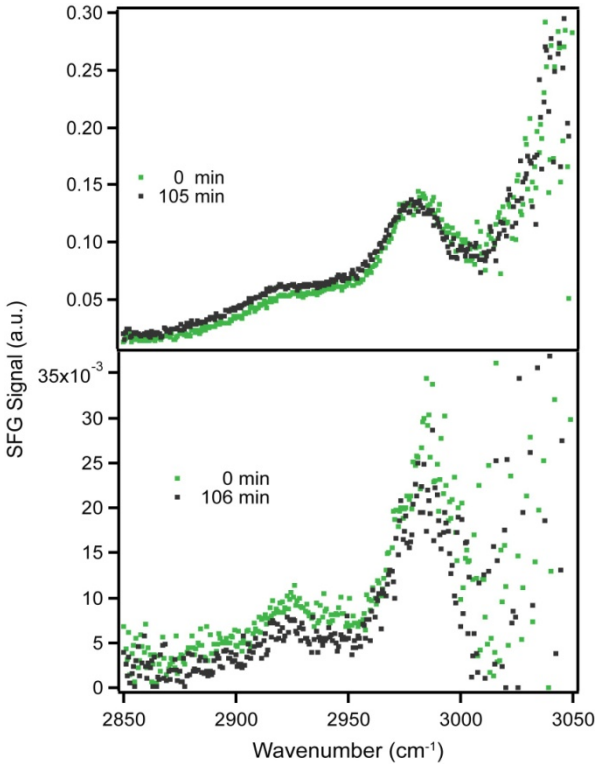

Figure 2.12 SFG ppp (top) and ssp (bottom) spectra of the C-H stretching region collected from a DPPC-d_{62}/DPPC-d_{62} bilayer in the Tris buffer over time.

2.4.2 Second harmonic generation experiments

As a complementary experiment, SHG was also used to monitor the PLD-induced hydrolysis reaction at the 1-palmitoryl-2-oleoyl-*sn*-glycero-3-phosphocholine (POPC) lipid bilayer. The SH signal was expected to change during the reaction since the interface potential of the lipid changes from neutral (POPC/POPC) to negatively charged (POPA/POPC).

2.4.2.1 Salt titration

One way to modulate the interfacial potential is to introduce a screening electrolyte. For example, adding sodium chloride to the silica/water interface at

pH values greater than the point of zero charge (pzc ~ 3) leads to a decrease in SHG as a result of the decrease in magnitude of the interfacial potential.[36] Figure 2.13 exhibits the change in the SH electric field as a function of salt concentration normalized to the SHG electric field from the Tris-buffer interface (50 mM Tris, 0 M NaCl, pH 8) for both bare silica and the supported POPC bilayer. Both interfaces exhibited an initial increase in SH electric-field upon adding salt, which we attribute to surface deprotonation by the sodium chloride.[36] Thereafter, the signal decreased at higher concentrations as screening took over. The extent of the decrease, however, varied for the two interfaces indicating that bare silica and the POPC/POPC bilayer interface interacted differently with the salt. Salt titration of a negatively charged surface, like bare silica in this case, was anticipated to lead to a more dramatic decrease in SHG compared with the zwitterionic lipid bilayer POPC/POPC interface with its net neutral charge. As expected, with the addition of sodium chloride in Tris-buffer (pH 8), the SHG intensity of the neutral POPC/POPC surface was less affected by the electrolyte solution. Importantly, these results confirmed that the zwitterionic POPC interface had a lower interfacial potential magnitude than the negatively charged bare silica, which indicated that the formation of the negatively charged phosphatidic acid should be discernable by the $\chi^{(3)}$ technique.

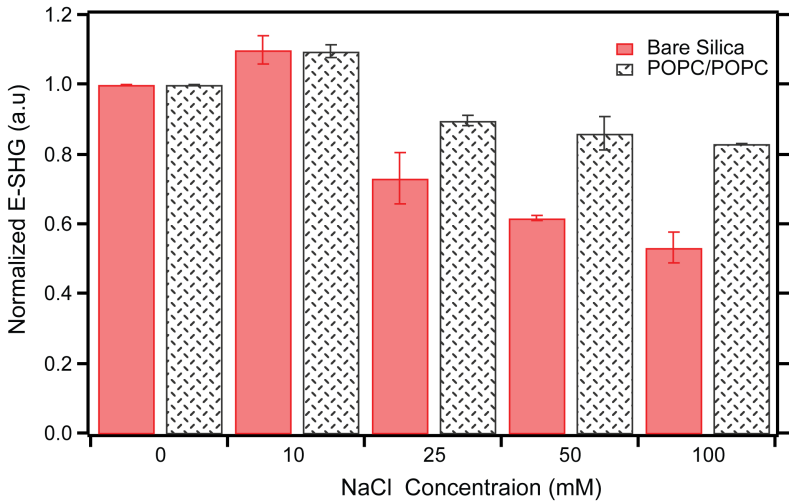

Figure 2.13 A comparison of titration curves for the POPC/POPC bilayer and bare silica with water interface in the presence of 0, 25, 50 and 100 mM NaCl in 50 mM Tris-buffer at pH 8.

2.4.2.2 PLD Assay

$\chi^{(3)}$ technique was used as a complementary nonlinear optical technique to investigate the reaction of PLD with a PC lipid bilayer. As SHG is directly proportional to the interfacial potential the increase in the surface charge that resulted from the cleavage of POPC by PLD should increase the signal. SHG data was collected at 295 nm, which avoided resonant enhancement detection of the lipase proteins ($\lambda < 270$ nm). As shown in Figure 2.14, the SHG intensity increased with time until 35 minutes, when the curve plateaued, indicating that the maximum amount of POPC was hydrolyzed to POPA and free choline. This experiment confirmed that $\chi^{(3)}$ was an alternative technique for monitoring enzymatic reactions that led to a change in the surface charge density.

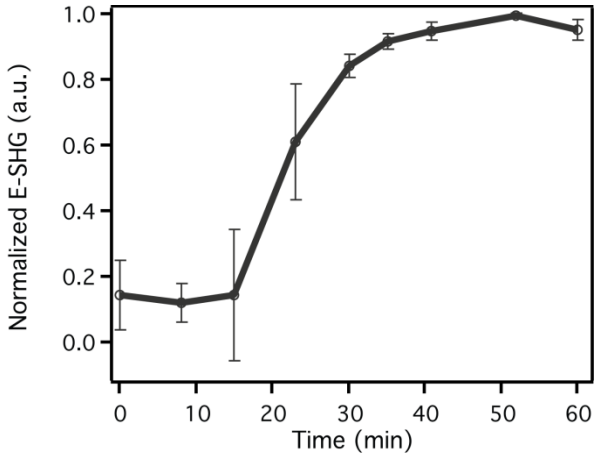

Figure 2.14 SHG intensity change with addition of PLD in Tris-buffer (pH 8) in the presence of 5 mM $CaCl_2$ at room temperature.

2.5 Conclusion

In conclusion, we have presented two methods for tracking PLD induced hydrolysis at the planar supported symmetric phospholipid bilayer. This investigation demonstrated that the head group of the bilayer can be monitored directly by SFG in the C-H stretching region. We observed an increase in signal, which we attribute to a break in inversion symmetry upon hydrolyzing the polar head groups in one leaflet. The significant decrease observed after the signal had reached a maximum supported previous work that the bilayer desorbed from the interface after reaction with PLD.[13] PLC induced hydrolysis also led to an increase in signal when a lower enzyme concentration or the non-optimal buffer were used. In contrast, when the optimal buffer and concentrated PLC were employed the signal immediately decreased, which we attribute to simultaneous hydrolysis of both leaflets. Additionally, it appeared that the PLC diacylglycerol product did not destabilize the lipid bilayer in contrast to the PLD phosphatidic acid product. This study provides insights into the different activities of PLD and

PLC with planar bilayers, and the stabilities of the hydrolysis product. Finally, the $\chi^{(3)}$ SHG technique was used as a complementary technique to probe the PLD-induced hydrolysis reaction on the planar surface since it changed the interfacial potential. This is the first observation of monitoring enzymatic reactions at bilayers with SHG, which could be extended to SHG microscopic imaging of enzymatic reactions at bilayers to gain spatial information.

2.6 Outlook

The work presented in this dissertation was motivated by the growing interest in understanding molecular interactions and their corresponding kinetics at biological interfaces. The application of VSFG to study model membranes has increased as a method for investigating a variety of biological processes. With its surface specificity, various important properties such as the phospholipid structure, orientation, and order can be directly probed at the membrane/water (buffer) interfaces. Although VSFG has led to a greater understanding of lipid dynamics and other processes involving interactions at bilayers, the requirement of an asymmetric bilayer (one protonated leaflet and one deuterated leaflet) has limited the VSFG investigations to model membrane systems. The phospholipase D induced hydrolysis reaction at a model phospholipid bilayers observed in this work provides direct experimental evidence for reactions at symmetric lipid bilayer. Consequently, other symmetric bilayers should be able to be monitored without using unnatural deuterated modifications. In addition, other membrane involved interactions, such as membrane-DNA interactions, and membrane-ion

interactions could be explored by directly monitoring the polar head group using our approach. Finally, as a follow up to this work, studies can be extended to investigate effects of temperature on phospholipase D-induced reaction of lipid bilayer, as well as stability of the product lipid bilayer under different conditions.

The results of the SHG studies can be used for the detection of molecule interaction on biological membranes without any labeling. The SHG study could be also extended to SHG microscopic imaging of enzymatic reactions at bilayers to gain spatial information. It holds promises for wide application in material science, biomedical science, bioengineering, and beyond.

2.7 Reference

1. Heller, A.; Koch, T.; Schmeck, J.; van Ackern, K., *Drugs* **1998,** *55* (4), 487-496.

2. Kassis, J.; Moellinger, J.; Lo, H.; Greenberg, N. M.; Kim, H. G.; Wells, A., *Clin. Cancer. Res.* **1999,** *5* (8), 2251-2260.

3. Gomez-Cambronero, J.; Keire, P., *Cell. Signal.* **1998,** *10* (6), 387-397.

4. Exton, J. H., *Physiol. Rev.* **1997,** *77* (2), 303-320.

5. Kim, I. H.; Lee, H. Y.; Lee, H. D.; Jung, Y. J.; Tendler, S. J. B.; Williams, P. M.; Allen, S.; Ryu, S. H.; Park, J. W., *Anal. Chem.* **2009,** *81* (9), 3276-3284.

6. Geng, D.; Chura, J.; Roberts, M. F., *J. Biol. Chem.* **1998,** *273* (20), 12195-12202.

7. Jenkins, G. M.; Frohman, M. A., *Cell. Mol. Life Sci.* **2005,** *62* (19-20), 2305-2316.

8. Hartono, D.; Bi, X. Y.; Yang, K. L.; Yung, L. Y. L., *Adv. Funct. Mater.* **2008,** *18* (19), 2938-2945.

9. Mills, G. B.; Moolenaar, W. H., *Nat. Rev. Cancer* **2003,** *3* (8), 582-591.

10. Bayburt, T.; Yu, B. Z.; Street, I.; Ghomashchi, F.; Laliberte, F.; Perrier, H.; Wang, Z. Y.; Homan, R.; Jain, M. K.; Gelb, M. H., *Anal. Biochem.* **1995,** *232* (1), 7-23.

11. Morris, A. J.; Frohman, M. A.; Engebrecht, J., *Anal. Biochem.* **1997,** *252* (1), 1-9.

12. Yamamoto, I.; Konto, A.; Handa, T.; Miyajima, K., *BBA-Biomembranes* **1995,** *1233* (1), 21-26.

13. El Kirat, K.; Dupres, V.; Dufrene, Y. F., *BBA-Biomembranes* **2008,** *1778* (1), 276-282.

14. Wu, H. L.; Yu, L.; Tong, Y. J.; Ge, A. M.; Yau, S.; Osawa, M.; Ye, S., *BBA-Biomembranes* **2013,** *1828* (2), 642-651.

15. Estrela-Lopis, I.; Brezesinski, G.; Mohwald, H., *Biophys. J.* **2001,** *80* (2), 749-754.

16. Gericke, A.; Huhnerfuss, H., *Chem. Phys. Lipids* **1994,** *74* (2), 205-210.

17. Grandbois, M.; Desbat, B.; Blaudez, D.; Salesse, C., *Langmuir* **1999,** *15* (19), 6594-6597.

18. Harper, K. L.; Allen, H. C., *Langmuir* **2007,** *23* (17), 8925-8931.

19. Ma, G.; Allen, H. C., *Langmuir* **2006,** *22* (12), 5341-5349.

20. Liu, J.; Conboy, J. C., *Langmuir* **2005,** *21* (20), 9091-9097.

21. Chen, X. Y.; Chen, Z., *BBA-Biomembranes* **2006,** *1758* (9), 1257-1273.

22. Anglin, T. C.; Liu, J.; Conboy, J. C., *Biophys. J.* **2007,** *92* (1), L1-L3.

23. Nguyen, K. T.; Le Clair, S. V.; Ye, S. J.; Chen, Z., *J. Phys. Chem. B* **2009,** *113* (36), 12358-12363.

24. Dicko, A.; Bourque, H.; Pezolet, M., *Chem. Phys. Lipids* **1998,** *96* (1-2), 125-139.

25. Liu, J.; Conboy, J. C., *J. Am. Chem. Soc.* **2004,** *126* (27), 8376-8377.

26. Liu, J.; Conboy, J. C., *Biophys. J.* **2005,** *89* (4), 2522-2532.

27. Tong, Y. J.; Li, N.; Liu, H. J.; Ge, A. L.; Osawa, M.; Ye, S., *Angew.Chem. Int. Edit.* **2010,** *49* (13), 2319-2323.

28. Hergenrother, P. J.; Haas, M. K.; Martin, S. F., *Lipids* **1997,** *32* (7), 783-788.

29. Tien, H. T.; Barish, R. H.; Gu, L. Q.; Ottova, A. L., *Anal. Sci.* **1998,** *14* (1), 3-18.

30. Chen, X. Y.; Clarke, M. L.; Wang, J.; Chen, Z., *Int. J. Mod Phys B* **2005,** *19* (4), 691-713.

31. Zhang, S. S.; Xu, L. L.; Zhao, X. W.; Chen, X.; Fan, Y. L.; Wan, Z. P.; Xu, Y. S.; Liu, W. L., *Plos One* **2013,** *8* (5).

32. Tamm, L. K.; Tatulian, S. A., *Q. Rev. Biophys.* **1997,** *30* (4), 365-429.

33. Ye, S. J.; Nguyen, K. T.; Le Clair, S. V.; Chen, Z., *J. Struct. Biol.* **2009,** *168* (1), 61-77.

34. Liu, J.; Conboy, J. C., *J. Am. Chem. Soc.* **2004,** *126* (29), 8894-8895.

35. Chen, X. Y.; Wang, J.; Kristalyn, C. B.; Chen, Z., *Biophys. J.* **2007,** *93* (3), 866-875.

36. Yang, P.; Wu, F. G.; Chen, Z., *J. Phys. Chem. C* **2013,** *117* (7), 3358-3365.

37. Brown, K. L.; Conboy, J. C., *J. Am. Chem. Soc.* **2011,** *133* (23), 8794-8797.

Chapter 3

Establishing the Generality of Lesion Induced DNA Amplification and Expanding This Method to RNA Detection

Portions of this chapter have been published. Kausar, A.; Mitran, C. J.; ***Li, Y****.; Gibbs-Davis, J. M., Angew.Chem. Int. Edit.* ***2013****, DOI: 10.1002/anie.201303225.*

Specifically, the experiments conducted on the ***DNA-I*** *sequence were performed by Abu Kausar and Catherine Mitran*

3.1 Introduction

3.1.1 Overview

Nucleic acids represent target biomarkers for many diagnostics aimed at detecting infectious diseases.[2,3,4] Especially, sequence-selective DNA/RNA detection has become increasingly important as it can be used to diagnose both infectious diseases and genetic diseases.[5,6,7] Since the target nucleic acid amount is usually very small, amplification of the nucleic acid sequence is critical for detection. Our group has recently developed an autonomous DNA self-replicating system that has potential in biodiagnostics.[8] In this chapter we discuss the generality of the system, and the expansion of this application for RNA detection.

3.1.2 Background and project goals

MicroRNAs (miRNAs) are single-stranded non-coding RNA molecules in length of 18–25 nucleotides. They play a critical role in many biological processes, such as cell differentiation, proliferation, tissue formation and cell death.[3,9,10] Diseases that change these processes are often associated with a change in cellular miRNA content. Several studies have shown that miRNAs are able to regulate the expression of tumor-associated genes.[11,12] Therefore RNA sequence-selective detection can be potentially used for diagnosing various early stages of human diseases as well as pathogen detection.[10,13] Most current techniques for sequence-selective RNA detection are based on the principle of base pair complementarity between a target RNA and one or more nucleic acid replicators. For example, in RNase protection assays (RPAs), this method involves

hybridization of target RNA to a complementary RNA probe, followed by digestion of nonhybridized probes with an RNase that specifically cleaves only single-stranded RNA but does not affect double-stranded RNA.[14,6,15] The dsRNA can then be analyzed by polyacrylamide gel. Although, this method offers direct RNA detection, it is time consuming and handling RNA probes could have potential limitations for point-of-care diagnosis. However, the most commonly used method is reverse transcription-polymerase chain reaction (RT-PCR). RT-PCR involves first transcribing the RNA target to a complementary DNA sequence using reverse transcriptase; this complementary DNA is then amplified by PCR and detected using standard methods. With the development of real time reverse transcription PCR (qRT-PCR) miRNA assays have achieved the detection of very small amounts of miRNA.[16,17,18] Although these methods offer high sensitivity, there are some restrictions confining the application of PCR-based assays. In particular, the requirement of thermal cycling instrumentation makes these assays expensive and difficult to implement in remote settings, hindering infectious disease monitoring in resource-limited parts of the world. Therefore, a sensitive assay that does not require a complicated replicator design and can be carried out isothermally is desired. In this chapter, we have developed an isothermal approach for detecting RNA by expanding the lesion induced DNA amplification method discovered in our lab so that it can be triggered by an RNA rather than DNA sequence.

The DNA self-replicating system that our group has developed is an isothermal DNA amplification system based on a ligase chain reaction (LCR)

using four primer sequences that is triggered in the presence of a target DNA strand. From our group's previous work, we found that introducing a model abasic destabilizing lesion (Ab), 1', 2'-dideoxyribose-5'-phosphate that consists of a sugar and phosphate group without the base in one of the primers, or replicators, was key to achieving amplification of DNA.[8] This early work established that the abasic group was compatible with ligation by T4 DNA ligase thereby facilitating isothermal DNA self-replication. In the first part of this chapter, we report how we achieve rapid sigmoidal amplification of DNA while avoiding the need for destabilizing enzymes or mechanical or thermal intervention using this common destabilizing abasic lesion and a high concentration of T4 DNA ligase. The generality of our method is studied using a target sequence associated with the Hepatitis B virus[19], which has a higher G:C content (**H-DNA-I**, shown in Table 1) than our original system.[1,8] The success of both systems and the simplicity of the replicator design suggests that this isothermal strategy will be accessible to many laboratories. This work also informs the development of an RNA template initiated DNA self-replication system that will be described later in the chapter.

The isothermal ligase chain reaction is cross-catalytic replication strategy involving two coupled catalytic cycles, four primers, or replicators, and the target strand to be replicated. The replication starts from the left cycle: two replicators, where one replicator contains a destabilizing abasic group in place of the complementary nucleotide at the 5'phosphate terminus, anneal to the complementary target **DNA-I** to form a nicked duplex. The nick is then ligated

with T4 DNA ligase (Figure 3.1A). The ligation product **DNA-II** is released due to the destabilizing effects of the central abasic nucleotide of the **DNA-II** on the product duplex (Figure 3.1A). The high concentration of the replicators drives the left cycle to continue and prevents the reannealing of the product duplex. Meanwhile, the released **DNA-II** is free to enter the right cycle. In this cycle, two additional replicators, both of which each contain half of the sequence of the target **DNA-I** while one contains a fluorescent label at the 5'phosphate terminus, anneal to the **DNA-II**, resulting in another nicked duplex (Figure 3.1 A'). Again, this nicked duplex undergoes ligation and dissociation (Figure 3.1 B' and C'). The released **DNA-II** continues in the right cycle, and the newly generated **F-DNA-I** that has the same sequence as the original target, but with the addition of a fluorescent label, serves as the template for the left cycle.[8] This feedback mechanism whereby the product of one cycle is the template for the other can lead to exponential amplification, which is critical for achieving the sensitivities need in biodiagnostic applications.

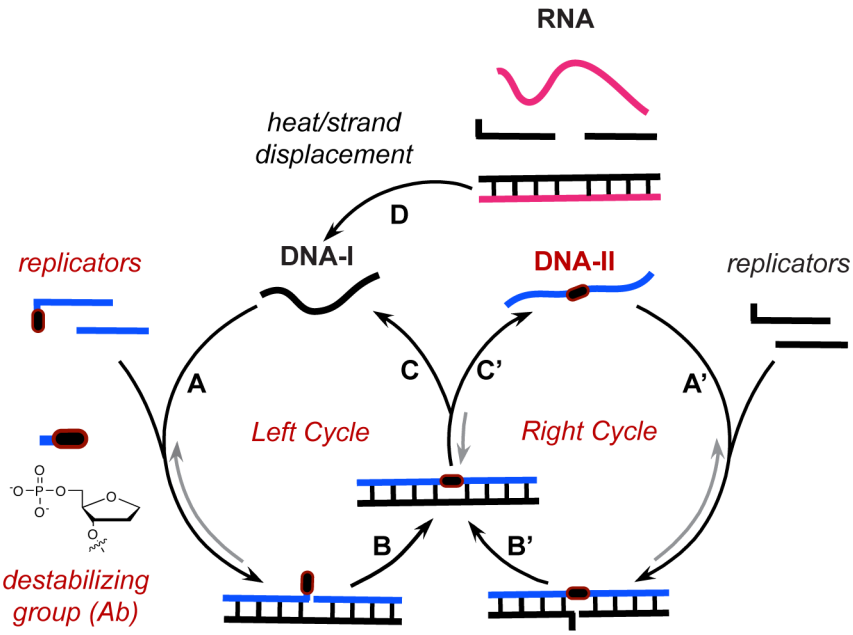

Figure 3.1 Schematic illustration of Cross-catalytic amplification of DNA-I target using an abasic destabilizing group in a ligase chain reaction. Left cycle: (A) Hybridization reaction between DNA-I and complementary replicators that contain a destabilizing group resulting a nicked duplex. (B) The nicked duplex is sealed by T4 DNA ligase resulting the product duplex. (C) The product duplex containing a DNA-I target and a ligation product DNA-II that incorporate a destabilizing group. This result the dissociation of the two strands. The replication continues as a result more formation and dissociation product duplex. Right cycle: (A') Hybridization reaction between DNA- II and complementary replicators. (B') The nicked duplex is sealed through ligation the same way as left. (C) Because of destabilization, the product duplex dissociates releasing a newly formed copy of DNA-I and the DNA-II strand. The new DNA-I strand feeds into the left cycle, while the DNA-II strand reenters the right cycle. (D) RNA detection can be achieved by incorporating another step into the DNA amplification system: two DNA replicators that are complementary to an RNA target are ligated in the presence of RNA and then dissociated by heating or by strand displacement. The released DNA-I is then amplified through the two DNA cross-catalytic cycles.

To achieve RNA detection, we contemplated developing a lesion-induced RNA amplification process using a mixture of DNA and RNA replicators. Unfortunately, the abasic 5'phosphate terminus is not compatible with RNA-templated DNA ligation using T4 DNA ligase. Therefore, we decided to introduce an extra step into the original DNA self replication assay such that the presence of

an RNA target leads to DNA amplification with T4 DNA ligase. Like in RT-PCR, this initial step should involve transcribing an RNA target to a complementary DNA sequence based on RNA-templated DNA ligation, using two replicators that are perfectly complementary to the RNA target (Figure 3.1D). Denaturing the ligated DNA product from the RNA template can be achieved by heating at 95 °C. Now, with the introduction of the four replicators one of which contains the destabilizing group, the complementary DNA product from the RNA templated step serves as the **DNA-I** template to achieve amplification isothermally (the same mechanism as the DNA self-amplification system). Therefore, RNA detection is accomplished by monitoring the formation of **DNA-I** with time. In the absence of target RNA, the RNA-templated DNA ligation will not proceed, which means there is no initial template for the DNA self-amplification cycle. Therefore, we should be able to distinguish between RNA initiated and no RNA initiated DNA self-replication.

3.2 Experimental section

3.2.1 Materials

Magnesium chloride hexahydrate ($MgCl_2 \cdot 6H_2O$) and Tris-base were purchased from Sigma. All the DNA oligonucleotides designed in this study were synthesized on an Applied Biosystems Model 392 DNA/RNA Synthesizer using standard phosphoramidite reagents and CPGs from Glen Research (Sterling, VA). The model abasic group was introduced with the dSpacer CE phosphoramidite (Catalog #10-1914). The 5'-end phosphate replicators were phosphorylated using

Chemical Phosphorylation Reagent II (Catalog #10-1902). The incorporation of the fluorescein labeled nucleotide was introduced either by using Fluorescein-dT phosphoramidite (Catalog #10-1056) or 6-Fluorescein phosphoramidite (Catalog #10-1964) at the 5'-end. All the DNA strands were deprotected and purified following the manufacture's protocol using the DMT-ON method with Glen-pak cartridges. The RNA oligonucleotides designed in this study and the RNAse free water used in all RNA experiments were purchase from Integrated DNA Technologies (Coralville, IA). The sequences of DNA and RNA oligonucleotides are listed in Table 3.1. Low-concentration T4 DNA ligase (1 unit/μL, Catalog #15224-017) and ligation buffer were purchased from Invitrogen. High-concentration T4 DNA ligase (2,000,000 cohesive end units/mL, catalog #M020T), ligation buffer, and ATP (10 mM, Catalog # P0756S) were purchased from New England Biolabs. All the water used in the DNA experiments was purified using a Millipore Milli-Q water system (18 MΩ, Milli-Q, Millipore). Reagents for polyacrylamide gel electrophoresis (PAGE), including 40% acrylamide mix solution and ammonium persulfate were purchased from BioRad Laboratories (Mississauga, ON, Canada). 2-Bis (dimethylamino)-ethane (TEMED) was purchased from Fisher Scientific (Nepean, ON, Canada).

Table 3.1 DNA and RNA sequences and modifications of H-DNA-I system, DNA-I system and E-DNA-I system.

H-DNA-I System			
H-DNA-I	5'-TATGGATGATGTGGTATT-3'	H-DNA-II_M	5'-AATACCAC***M'***TCATCCATA-3'
H-rDNA-Ia	5'-$_F$TATGGATGA-3'	H-rDNA-IIa	5'-$_P$***M'***TCATCCATA-3'
H-rDNA-Ib	5'-$_P$TGTGGTATT-3'	H-rDNA-IIb	5'-AATACCAC -3'
		H-rDNA-IIb'	5'-$_F$ AATACCAC -3'
DNA-I System			
DNA-I	5'-TTGTTAAATATTGATAAG-3'	DNA-II_M	5'-CTTATCAA***M***ATTTAACAA-3'
rDNA-Ia	5'-$_F$TTGTTAAAT-3'	rDNA-IIa	5'-$_P$***M***ATTTAACAA-3'
rDNA-Ib	5'-$_P$ATTGATAAG-3'	rDNA-IIb*	5'-$_F$CTTATCAA-3'
E-rDNA-Ib	5'-$_P$***M'***TGATTCCAT-3'	E-rDNA-IIb'	5'-$_F$ATGGAATCA -3'
E-DNA-I System			
E-RNA-I	5'-UUGUUCGAUUGAUUCCAU-3'	E-DNA-II	5'-ATGGAATCAATCGAACAA-3'
E-DNA-I_M	5'-TTGTTCGA***M'***TGATTCCAT-3'	E-rDNA-IIa	5'-$_P$ATCGAACAA-3'
E-rDNA-Ia	5'-T_FTGTTCGA-3'	E-rDNA-IIb	5'-ATGGAATCA -3'
E-rDNA-Ib	5'-$_P$***M'***TGATTCCAT-3'	E-rDNA-IIb'	5'-$_F$ATGGAATCA -3'

rDNA = replicator DNA sequences; F = fluorescein, M' = Abasic or A; P = phosphate.

3.2.2 Instrument

The DNA was synthesized on an Applied Biosystems Model 392 DNA/RNA Synthesizer. MALDI-MS was performed on a Voyager Elite (Applied BioSystems, Foster City, CA) time of flight-mass spectrometer in linear negative

mode. All the DNA and RNA ligation experiments were conducted under a Torrey Pines Scientific Echotherm Chilling/Heating Plate Model IC22 with desired temperatures. The 15% polyacrylamide gel electrophoresis (PAGE) gels was performed using the Bio-Rad Mini-PROTEAN Tetra Cell System to determine the ligated product. The gels were imaged using ImageQuant RT ECL Imager from GE Healthcare Life Science using UV transillumination. Melting analyses of DNA-containing materials were performed using an HP 8453 diode-array spectrophotometer equipped with a HP 89090A Peltier temperature controller, and the melting curves were analyzed with ChemStation software.

3.2.3 Ligation experiment

The final buffer composition for all DNA ligation reactions was 50 mM Tris-HCl (pH 7.5), 10 mM $MgCl_2$ and 1 mM ATP. The single cycle DNA ligation reaction was performed as follows: single-strand DNA target (**H-DNA-I** or **H-DNA-II**; final concentration 1.4 μM), florescent replicator (final concentration 1.4 μM) and the phosphate-terminated replicator (final concentration 2.8 μM) were combined. To this mixture was added 1 unit of T4 DNA ligase and master mix to react a total volume of 15 μL. The reaction mixture was then incubated at 26 °C and monitored at different times. To determine the amount of ligation product as a function of time, 3-μL aliquots were removed and mixed with 1 μL of 0.5 M EDTA solution to stop ligation.

The typical cross-catalytic cycle DNA ligation reaction was performed as follows: single-strand DNA target (**H-DNA-I**; final concentration 14 nM-1.4 pM),

fluorescent replicator (final concentration 1.4 μM) and the three other replicator strands (final concentration 2.8 μM) were combined and incubated at the desired temperature. To this mixture was added 2,000 cohesive end units of T4 DNA ligase and master mix to reach a total volume of 15 μL. The ligation mixture was allowed to react in the heat block at the desired temperature and aliquots were taken at various times by the same manner as described earlier.

The final buffer composition for all RNA ligation reactions was 50 mM Tris-HCl (pH 7.5), 10 mM $MgCl_2$, 10 μM ATP. Typical RNA detection experiments were performed following two steps: In the first step, RNA target (**E-RNA-I**, final concentration 14 nM-14 pM) was incubated with two DNA replicators (**E-DNA-IIa** and **E-DNA-IIb**, final concentration 2.8 μM) which are complementary to the RNA target, T4 DNA ligase (1,650 cohesive end units) was added to this mixture to reach a final volume of 7.5 μL. The RNA-templated ligation was carried out for two hours at 26 °C. In the second step, the ligation mixture was denatured for 10 minutes at 95 °C, the 5'-abasic phosphate-labeled DNA replicator (**E-DNA-Ib**, final concentration 2.8 μM) and 5'- fluorescein-labeled DNA replicator (**E-DNA-Ia**, final concentration 1.4 μM) were then added to this mixture and allowed to anneal for 5 minutes at 37 °C, followed by 3,300 cohesive end units of T4 DNA ligase to reach a total volume of 15 μL. This reaction was carried out in a buffer containing less ATP (50 mM Tris-HCl, pH 7.5, 10 mM $MgCl_2$ and 1 mM ATP) at 37 °C.

3.2.4 Determination of turnover

The ligated products on the polyacrylamide gel electrophoreses (PAGE) can be determined using ImageQuant RT ECL Imager by quantifying the ratio of fluorescein-labeled replicators to fluorescein-labeled ligated product based on the following equation:

$$\%\ ligated\ product = \frac{I_{product}}{I_{product}+I_{reactant}} \times 100\% \quad (3.1)$$

The concentration of the ligated product can be calculated by the percentage of the ligated product multiplied by the concentration of the fluorescently labeled replicator (the limiting replicator).

The number of the net replication cycles for a typical cross-catalytic ligation reaction can be calculated using following equation:

$$Replication\ Cycles = \frac{\%\ yield_{templated\ ligation} - \%\ yield_{non-templated\ ligation}}{[template\ DNA]}[limiting\ replcator] \quad (3.2)$$

Again, the fluorescent-labeled replicator is the limiting replicator, which is the half concentration of the other replicators and the template concentration in the following experiment are from 14 nM to 14 pM.

3.2.5 Melting experiments

The melting temperature (T_m) is the temperature at which 50% of the DNA duplexes are denatured and is a common parameter for assessing DNA duplex stability. The relative amount of single- or double-strand DNA in solution can be

determined experimentally by ultraviolet absorbance spectroscopy at the absorbance wavelength of 260 nm (OD_{260}). Due to hypochromicity, double stranded DNA absorbs less than that of single stranded DNA, therefore the difference of absorbance at 260nm can be measured as a function of temperature to monitor thermal duplex dissociation. In a typical melting experiment, 1.3 nmol of each DNA strand is combined in buffer (10 mM PBS, pH 7, 20 mM $MgCl_2$) with a final volume of 1mL. The resulting mixture was annealed by heating to 95 °C followed by slow cooling for 1 hour. The DNA melting curve was determined using an HP 8453 diode-array spectrophotometer, equipped with a HP 89090A Peltier temperature controller. The melting experiments were performed in 1 cm pathlength quartz cells and stirred at 100 rmp. The temperature was varied from 10 to 80 °C, with 1°C temperature increment and 1 minute hold time. The absorbance at 260 nm was monitored and baseline corrected with the absorbance at 350 nm. Melting temperatures were determined from the maximum of the first derivative of the melting transition analyzed with ChemStation software.

3.2.6 MALDI-TOF characterization of the synthesized oligonucleotides

The DNA strands used in this study were characterized by MALDI-TOF. 1 nmol DNA sample was dissolved in triethylamine acetate buffer (0.1 M TEAA, pH 7.0) and desalted by a standard desalting procedure using C18 Zip-tip pipette tips (ZipTip, Millipore). The DNA was eluted from the ZipTip with 5 μL of matrix/ammonium citrate solution by repeating aspiration and dispersion three

times and dispensing the sample into a microcentrifuge tube. The desalted DNA/matrix/ammonium citrate solution (0.6 to 1 μL) was spotted on a MALDI plate and allowed to dry. MALDI-MS was then performed on a Voyager Elite time of flight-mass spectrometer in linear negative mode. Bovine insulin and Bovine insulin chain B were used to calibrate the instrument. The calculated mass and the found mass are as following: **H-DNA-I**: calculated mass, 5600; measured, 5600. **H-rDNA-Ia (fluorescein-modified)**: calculated mass, 3290; measured, 3293. **H-rDNA-Ib (5'-phosphate):** calculated mass, 2840; measured, 2841. **H-DNA-II, *M* = *A***: calculated mass, 5396; measured, 5395. **H-DNA-II, *M* = *Ab***: calculated mass, 5263; measured, 5263. **H-rDNA-IIa, *M* = *Ab* (5'-phosphate)**: calculated mass, 2918; measured 2920. **H-rDNA-IIa, *M* = *A* (5'-phosphate)**: calculated mass, 3051; measured, 3051. **H-rDNA-IIb**: calculated mass, 2363; measured, 2363.

3.3 Results and discussion

3.3.1 Melting temperature determination of the H-DNA-I system

Using a combination of high concentration of T4 DNA ligase and a destabilizing lesion, our group demonstrated that self replication could happen rapidly for an 18 base sequence that was A:T rich (**DNA-I** system, Table 3.1)[1]. My goal was to determine if this self-replication strategy was general and could be used to amplify target sequences with greater G:C content. Consequently, I developed a similar system to the original DNA-I that was specific to an 18 base sequence unique to the Hepatitis B virus (**H-DNA-I**). One of the important

parameters for this isothermal self-replication system is the stability between the replicators and the target DNA (nicked duplex) compared with that of the corresponding ligated product and the target DNA (product duplex). The thermal dissociation, or melting, temperature (T_m) is a straightforward parameter to evaluate and compare the stability of each component of our system. From the resulting melting curves (Figure 3.2) and T_m values (Table 3.2) for the hepatitis B system, the T_m corresponding to the perfectly complementary duplex (**H-DNA-I**: **H-DNA-II$_A$**) was found to be 55.4 $^{\circ}$C, whereas the T_m value of an abasic group incorporated into the DNA duplex (**H-DNA-I**: **H-DNA-II$_{Ab}$**) was 43.8 $^{\circ}$C. This result suggested that the incorporation of the abasic into the middle of the DNA duplex decreased the T_m of the ligated product duplex significantly (ΔT_m =11.6 $^{\circ}$C). The nicked duplexes exhibited a similar trend but the magnitude of the difference was much smaller. For example, the T_m value of the nicked duplex from the left cycle: with perfect complementary replicators (**H-DNA-I**: **H-rDNA-II$_A$**: **H-rDNA-II$_b$**) and with abasic incorporated complementary replicators (**H-DNA-I**: **H-rDNA-II$_A$**: **H-rDNA-II$_{Ab}$**) was 20.7 ^{o}C and 20.2 ^{o}C, respectively. The T_m value of the nicked duplex from the left cycle: with perfect complementary replicators (**H-DNA-II**: **H-rDNA-I$_a$**: **H-rDNA-I$_b$**) and with abasic incorporated complementary replicators (**H-DNA-II$_{Ab}$**: **H-rDNA-Ia**: **H-rDNA-I$_b$**) were 28.6 °C and 22.6 °C, respectively. It is unclear why the nicked duplex of the right cycle is more destabilized by the destabilizing group than that of the left cycle. Most importantly, these results reveal that the destabilizing group decreased the stability difference between the product duplex and the nicked duplexes compared

with the perfectly complementary system as the destabilizing group had a larger effect on the product duplex. Comparing the melting temperatures of the product duplex with the least stable nicked duplex leads to a ΔT_m of 34.7 °C and 23.6 °C for the perfectly complementary and abasic containing systems, respectively. By bringing their melting temperatures closer together, the destabilizing group provided a temperature where both the nicked duplex and product duplex were stable but labile, which is key to achieving turnover in the replication cycle.

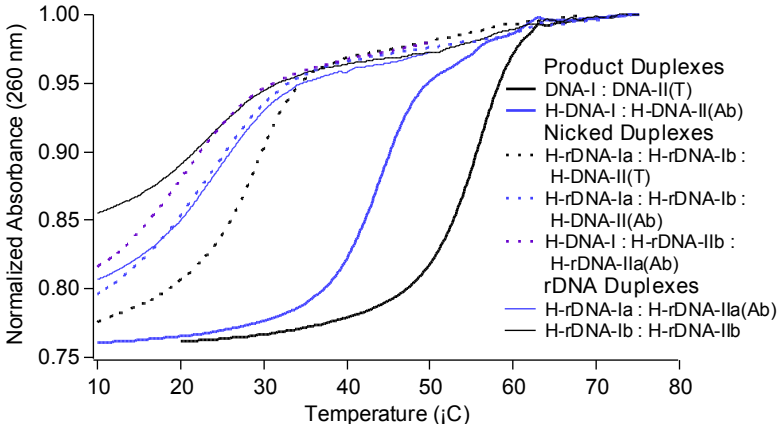

Figure 3.2 Melting profiles of the H-DNA-I and DNA-I system corresponding to the product duplex, nicked duplex and the replicator (rDNA) duplexes.

The trends in T_m values were similar for the **DNA-I** system (work done by my colleague Abu Kausar). Specifically, the ΔT_m of the product duplex with the least stable nicked duplex was 31.9 °C and 20.6 °C for the perfectly complementary and abasic containing systems, respectively. From the thermal denaturation experiments, both **H-DNA-I** and **DNA-I** systems revealed that incorporating an abasic group into the middle of a DNA strand destabilizes the ligated product duplex. Therefore, in the self-replication system, the ligation

product can be released from the DNA templates; owing to destabilization both of the two strands can serve as templates and continue the self-replication cycle isothermally in the left cycle and right cycle.

Table 3.2 Melting temperatures (T_m) of duplexes formed during cross-catalytic replication of H-DNA-I system and DNA-I system.

DNA-I System		**H-DNA-I System**	
Mixture	**T_m (°C)**	**Mixture**	**T_m (°C)**
DNA-I:DNA-II *(M = T)*	49.2	H-DNA-I:H-DNA-II (*M' = T*)	55.4
DNA-I:DNA-II *(M = Ab)*	34.0	H-DNA-I:H-DNA-II (*M' = Ab*)	43.8
DNA-I:rDNA-IIa:rDNA-IIb *(M = T)*	17.3	*H-DNA-I:H-rDNA-IIa:H-rDNA-IIb (M' = A)*	20.7
rDNA-Ia:rDNA-Ib:DNA-II *(M = T)*	22.8	H-rDNA-Ia:H-rDNA-Ib:H-DNA-II *(M' = A)*	28.6
rDNA-Ia:rDNA-Ib:DNA-II *(M = Ab)*	13.4	H-rDNA-Ia:H-rDNA-Ib:H-DNA-II *(M' = Ab)*	22.6
DNA-I:rDNA-IIa:rDNA-IIb *(M = Ab)*	16.4	H-DNA-I:H-rDNA-IIa:H-rDNA-IIb *(M' = Ab)*	20.2
rDNA-Ia:rDNA-IIa *(M = Ab)*	12.8	H-rDNA-Ia:H-rDNA-IIa *(M' = Ab)*	23.9
rDNA-Ib:rDNA-IIb	13.3	H-rDNA-Ib:H-rDNA-IIb	22.8

3.3.2 Temperature optimization of cross-catalytic replication of H-DNA-I

T4 DNA ligase catalyzes the formation of a phosphodiester bond between 5'-phosphate and 3'-hydroxyl termini in the presence of the DNA template. To monitor this process, we utilized denaturing polyacrylamide gel electrophoresis (PAGE). Using fluorescent imaging and one fluorescently labeled replicator out of the four types of replicators present, a single cycle experiment was performed

using **H-DNA-I** was a template and monitoring the formation of the destabilized complement with time. The top band in the gel was attributed to the ligated product band (**F-H-DNA-II$_{Ab}$**) and the bottom band the reactant band (**H-rDNA-IIb'**) (Figure 3.3E). As shown after 10 min all the reactant was consumed forming the ligated product when 1 equivalent of the **H-DNA-I** with respect to the fluorescent replicator was present. The control experiment also showed that without added **H-DNA- I** template, even in the presence of T4 DNA ligase, the ligation did not proceed.

The ideal replication temperature must balance many competing parameters. On the one hand, the replication temperature should not be too far above the T_m of the nicked duplex. On the other hand, the replication temperature should not be too far below the T_m of the product duplex in order to overcome product inhibition. No doubt these two conditions have to reach a compromise in order to achieve isothermal turnover. To determine the ideal replication temperature, a series of temperature studies on **H-DNA- I** system were carried out. Each cross-catalytic replication was performed with two parallel runs initiated by 14 nM and 0 nM **H-DNA-I** template. The difference between the templated-reaction and nontemplated reaction (control) were compared at each time point. Figure 3.3 shows the cross-catalytic replication carried out at 30, 34 and 37 °C. The data revealed that the rate of reaction was fastest at 37 °C, and the reaction went to completion at 50 minute. However, very little discrimination of the templated reaction and non-templated reaction was found. Instead the optimized temperature for this system was found to be 34 °C as it gave a

distinguishable separation between the templated reaction and nontemplated reaction at a relatively short time frame. The optimized reaction temperature for the **DNA- I** system was at 30 °C.[1] The higher optimal temperature for the **H-DNA-I** system can explained by the greater G:C content of the **H-DNA-I** system than **DNA- I** system, also revealed by the higher T_m of the **H-DNA-I** system. In the following sections, all the **H-DNA- I** experiments were conducted at 34 °C.

Comparing the temperature variation studies with the T_m values determined in the melting experiments indicated that the ideal replication temperature was 10 °C below the T_m of the product duplex and 8 °C above the T_m of the fragment:template nicked duplexes for the **H-DNA-I** system (T_m values correspond to 1.3 nM per sequence). For the **DNA-I** system the same relative temperature dependence was observed with the optimal replication temperature lying 4 °C below the T_m of the product duplex and ~15 °C above the melting temperature of the corresponding fragment:template nicked duplexes. We conclude that the ideal temperature was great enough to facilitate product duplex dissociation yet still resulted in the formation of some nicked duplexes. Importantly, the more concentrated T4 DNA ligase compensated for the small amount of nicked duplexes present at this temperature.

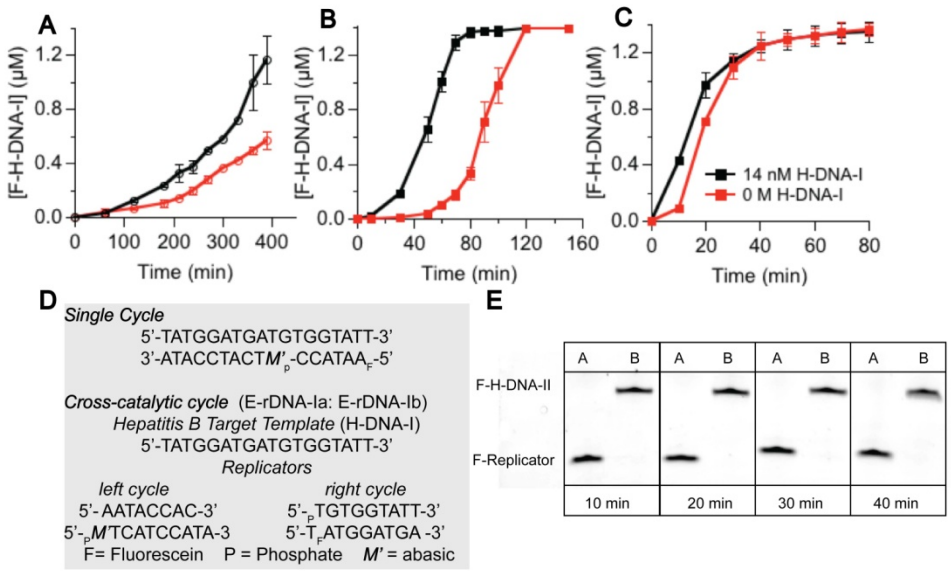

Figure 3.3 The concentration of F-H-DNA-I formed as a function of time using an abasic modified replicator at (A) 30 °C, (B) 34 °C, and (C) 37 °C. The black traces correspond to the experiment initiated with 14 nM H-DNA-I and the red traces correspond to the experiment initiated with no H-DNA-I. *Experimental conditions:* 14 nM H-DNA-I; 1.4 μM H-rDNA-Ia; 2.8 μM H-rDNA-Ib; 2.8 μM H-rDNA-IIa (*M' = Ab*); 2.8 μM H-rDNA-IIb. (D) Sequences corresponding to the cross-catalytic cycle with Hepatitis B template. (E) Single cycle (left) at 26 °C initiated by 1.4 μM and 0 μM H-DNA-I using destabilizing fragments (*M' = Ab*), one of which possesses a fluorescein, leading to the formation of the fluorescently labeled complement (F-H-DNA-II_{Ab}).

We found that both the reactions with and without any initial **H-DNA-I** exhibited sigmoidal growth for the cross-catalytic cycle experiment (Figure 3.3B). Whereas in the single cycle experiment, when no initial **H-DNA- I** was present, no product was formed (Figure 3.3D). In the cross-catalytic system, the two replicators from the left cycle are complementary with the two replicators from the right cycle. Therefore, the ligated product can be formed via pseudo-blunt-end ligation of the fragments in the presence of T4 DNA ligase.[20] (The reaction is pseudo-blunt end as there is a non-complementary one-base overhang, pairing an thymine across from an abasic group). The small quantities of **F-H-DNA-I** or **H-**

DNA-II$_{Ab}$ generated in this slow background process could then trigger cross-catalytic replication. Fitting the sigmoidal logistic growth function f(t) = a/(1 + be^{-ct}) to the data plotted in Figure 3.3B allowed us to quantify the rate of replication, where *a* is the maximum concentration of **F-DNA-I** formed, *b* is the extent of sigmoidicity and *c* is the exponential rate. We observed that the rates were the same within error for the target-initiated and background reactions (0.10 ± 0.02 min^{-1}, corresponding to a doubling rate every 7 minutes).

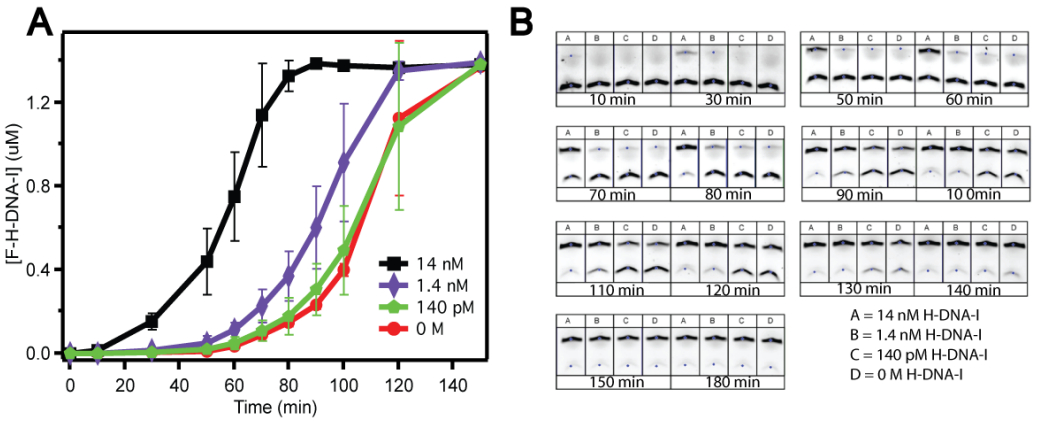

Figure 3.4 The concentration of F-H-DNA-I formed as a function of time using an abasic modified replicator at 34 °C with different concentrations of template. (A) The black traces correspond to the experiment initiated with 14 nM H-DNA-I and the red, green and purple traces correspond to the experiment initiated with 0n M, 140 pM and 1.4 nM H-DNA-I. The condition of Replicators for all experiments listed remains the same. *Replicator conditions:* 1.4 µM H-rDNA-Ia; 2.8 µM H-rDNA-Ib; 2.8 µM H-rDNA-IIa (*M' = Ab*); 2.8 µM H-rDNA-IIb. (B) The representative gel image corresponding to the experiment.

3.3.3 Replicator concentration optimization of cross-catalytic replication of H-DNA- I

We have successfully proven our isothermal self-replication system is general for an 18-base DNA detection. However, the challenge for a DNA

detection system is to improve the sensitivity, which in this case is try to find a way to delay the non-templated reaction. Various concentrations of **H-DNA-I** target were used to the same concentration of the replicators as shown in Figure 3.4. The clear discrimination between the templated reaction and non-templated ligation were observed at **H-DNA-I** template concentrations of 14 nM and 1.4 nM. In contrast, when the reaction was initiated with **H-DNA-I** concentrations lower than 1.4 nM, such as 140 pM, the discrimination was unnoticeable.

With template concentrations less than 1.4 nM, the replication profile mirrored that of the non-templated reaction. Consequently, we developed an assay that used the current system but lowered the concentration of the replicators. In this way, our results showed that 140 pM of initial **H-DNA- I** template could be detected (Figure 3.5). And there is a detectable difference in signal at even lower concentration of the **H-DNA- I** template.

Each concentration was tested three times (n = 3). The plot in Figure 3.6A results from the combination of Figure 3.4A and Figure 3.5A. It reveals that the rate of replication was slower with the lower concentration of the DNA replicators; however, with one-fourth the standard replicator concentration, we were able to detect the DNA template up to 14 pM by slowing down the background reaction more so than the templated reaction.

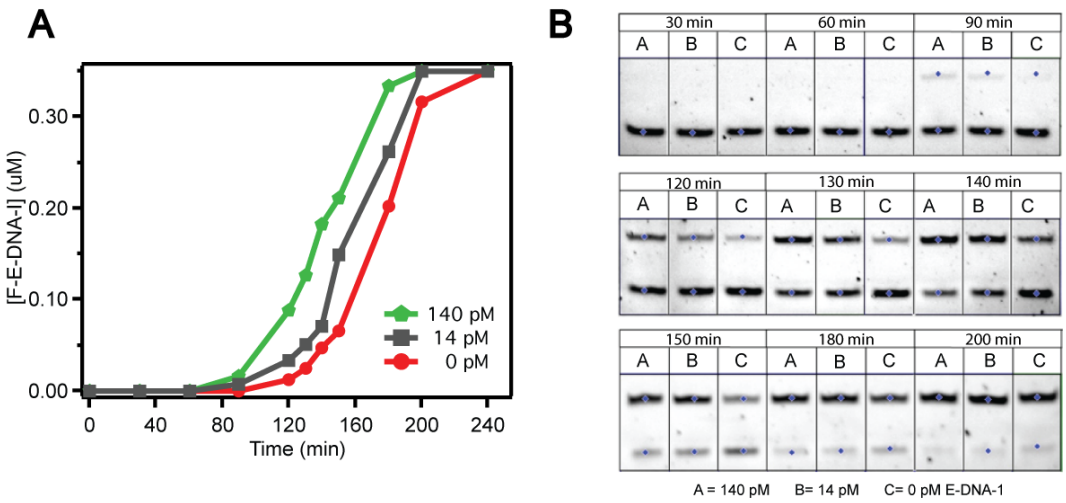

Figure 3.5 The concentration of F-H-DNA-I formed as a function of time using an abasic modified replicator at 34 °C with different concentrations of template. (A) The grey traces correspond to the experiment initiated with 14 pM H-DNA-I and the red, green and purple traces correspond to the experiment initiated with 0n M, 140 pM H-DNA-I. The condition of Replicators for all experiments listed remains the same. *Replicator conditions:* 0.35 µM H-rDNA-Ia; 0.7 µM H-rDNA-Ib; 0.7 µM H-rDNA-IIa (*M' = Ab*); 0.7 µM H-rDNA-IIb. (B) The representative gel image corresponding to the experiment.

To evaluate the extent of turnover in the replication process, we determined the number of net replication cycles from the concentration of **F-H-DNA-I** formed divided by the initial **H-DNA-I** concentration. Figure 3.6B illustrates the turnover of the target (template) at 14 nM, 1.4 nM, 140 pM and 14 pM. With 140 pM template, we measured 920 ± 50 replication cycles. And with 14 pM template, 6000 ± 600 replication cycles can be observed. The number of net replication cycles for each experiment were calculated as shown in table 3.3. We observed that the lower the template concentration, the more replication cycles were obtained.

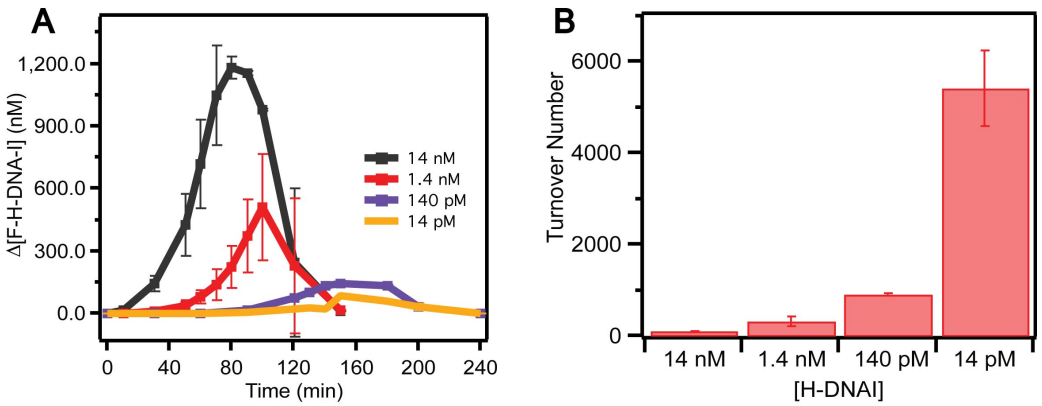

Figure 3.6 The concentration of F-H-DNA-I formed as a function of time using an abasic modified replicator at 34 °C with different concentrations of template and replicators (A) The purple, yellow, black and green traces correspond to the experiment initiated with 14 nM, 1.4 nM, 140 pM and 14 pM H-DNA-I. The condition of replicators for purple and yellow traces remains the same: 1.4 μM H-rDNA-Ia; 2.8 μM H-rDNA-Ib; 2.8 μM H-rDNA-IIa (*M' = Ab*); 2.8 μM H-rDNA-IIb. The condition of replicators for green and black traces remains the same: 0.35 μM H-rDNA-Ia; 0.7 μM H-rDNA-Ib; 0.7 μM H-rDNA-IIa (*M' = Ab*); 0.7 μM H-rDNA-IIb. (B) The Turnover number of F-H-DNA-I with ligation initiated with 14 nM, 1.4 nM, 140 pM and 14 pM H-DNA-I.

3.3.4 Conclusion

In conclusion, based on my Group's established system that replacing one nucleotide with an abasic group allows DNA to isothermally self-replicate in a ligase chain reaction. Based on the success of the Hepatitis B target using this approach, it appears this strategy is general for 18-base DNA target detection. Moreover, this system was found to be optimized at 34 °C and the detection limit was 14 pM. Importantly, this strategy required neither complicated design of the replicators nor sophisticated instruments, and it took less than 4 h to finish an assay. Compared with the traditional DNA sensing strategy, the method is simple, thereby representing a good isothermal signal amplification scheme.

Table 3.3 Maximum new amount of F-H-DNA-I formed during cross-catalytic replication as a function of initial template concentration.

# of Run	[**H-DNA-I**]	[**F-H-DNA-I**] Formed (nM)		Δ[**F-H-DNA-I**] Formed (nM)	Net Replication Cycles		Time (min)
		With Template	Without Template			Average	
I		1,370	152	1,220	87.2		90
II		1,390	216	1,170	84.1		90
III		1,310	213	1,100	78.5		90
IV	14 nM	1,400	186	1,210	86.6	85±3	90
V		1,400	191	1,210	86.2		90
VI		1,380	169	1,210	86.8		90
VII		1,340	177	1,160	82.9		90
I		733	290	443	317		100
II		711	382	330	236		100
III	1.4 nM	691	294	397	284	310±50	100
IV		767	296	471	336		100
V		778	266	512	366		100
I		201	76.3	124	888		130
II	140 pM	171	46.6	125	891	920±50	130
III		173	37.3	135	970		140
I		209	118	91	6500		140
II	14 pM	189	114	74	5300	6000±600	140
III		147	62	85	6100		150

The Experiments with 140 and 14 pM template were done with four-fold diluted replicator.

3.4 Development of RNA-initiated lesion induced DNA amplification (LIDA)

3.4.1 The ATP concentration optimization of RNA-templated DNA ligation

In order to apply lesion induced destabilization amplification (LIDA) to RNA detection a two-step replication system has been designed and investigated (Figure 3.1). In the first step, RNA-templated DNA ligation is used to translate the RNA to the complementary DNA sequence using T4 DNA ligase, the same enzyme utilized in the amplification steps. Figure 3.7 exhibits the rate of DNA ligation in the presence of one equivalent of the complementary RNA template

(1.4 μM) at 26 °C. The reactions were conducted under three different concentrations of ATP. The DNA-templated DNA ligation is usually performed at the ATP concentration at 1 mM, and we observe no ligated product after 20 hours for RNA-templated DNA ligation (Figure 3.7A, ii). By decreasing the ATP concentration by one order of magnitude (100 μM), we started to see the ligated product after 20 hours, and with an ATP concentration of 10 μM, the reaction was complete after this amount of time (Figure 3.7A, iv and vi, respectively).

This result confirmed that RNA-templated DNA ligation needed more enzyme and a lower concentration of ATP in comparison with the DNA-templated reaction. According to the Landegren group and others, the reaction mechanism of the T4 DNA ligase-catalyzed sealing of nicked DNA substrates can explain this phenomenon.[3,17,18] The T4 DNA enzyme is activated through ATP hydrolysis, resulting in the enzyme being covalently bonded to an AMP. As the T4 ligase-AMP binds to the 5'-phosphate ligation site of a nicked DNA duplex, the enzyme transfers this AMP to the phosphorylated 5'-end at the nick, producing an intermediate substrate attached through a 5'-5' pyrophosphate bond. The OH group at the 3'-end of the nick attacks the 5'-5' pyrophosphate bond of the intermediate, resulting in the product and causing the ligase and AMP to be released. The released ligase is then further recharged with AMP forming the enzyme-ATP intermediate and catalyze more ligations. However, if the ligase prematurely releases from the nicked duplex before the 3'-OH attach to it, then the 5' AMP is accumulated at the 5'-end permanently, blocking further ligation

attempts. Therefore, the ATP concentration for this RNA-templated DNA ligation is critical and essential in this enzymatic reaction processes.

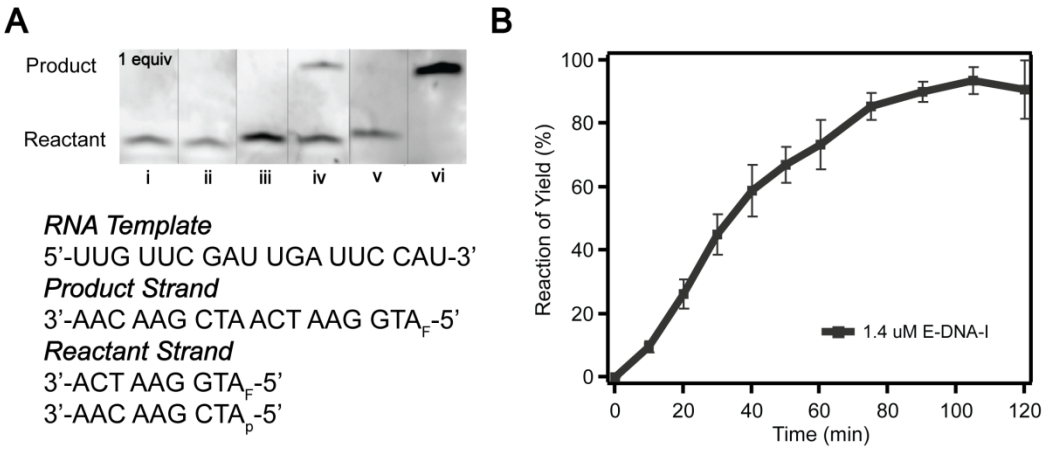

Figure 3.7 The study of single-cycle RNA-templated DNA ligation at 26 °C. (A) PAGE image illustrating the amount of ligated DNA product formed in 20 hours without (i, iii, v) and with (ii, iv, vi) RNA template as a function of different ATP concentrations: i and ii: 1000 μM ATP; iii and iv: 100 μM ATP; v and vi: 10 μM ATP. (B) A time-course of ligation of the DNA reactant strands in the presence of RNA template with 10 μM ATP. *Experimental conditions:* (1 equiv = 1.4 μM) RNA template (E-DNA-I) 0 or 1 equiv; fluorescent reactant strand (E-rDNA-IIb') 1 equiv; 5'-phosphate reactant strand (E-rDNA-IIa) 2 equiv; ligation buffer (10 mM Tris-HCl pH 7.5, 10 mM $MgCl_2$ and varying ATP); 1650 units T4 DNA ligase/7.5 mL.

3.4.2 Replicator concentration optimization of RNA-initiated LIDA

Figure 3.8 b illustrates the time-course study of ligation of the DNA replicators (reactant strands) with the RNA template. After 120 min, the reaction was more thatn 95% complete. Therefore, 120 min reaction time was used for the RNA-templated DNA ligation step prior to DNA amplification. This first step was also carried out with the optimized ATP concentration of 10 μM.

In the second step the transcribed DNA which is complementary to the RNA target further serves as a template in the cross-catalytic self replication strategy in the presence of four DNA replicators (two of the DNA replicators contains the sequences of the corresponding RNA sequences but with the addition of an abasic group at the 5'-end). We note that efforts to incorporate the destabilizing group into the replicators used in the first step involving RNA-templated ligation were not successful.

As shown in the Figure 3.8A, similar to the DNA-initiated system, we observed rapid sigmoidal amplification of DNA using RNA to initiate the process. At concentrations of 14 nM RNA template, the reaction proceeded faster than in the absence of template (Figure 3.8A). In these experiments, the RNA-templated reaction was allowed to react for 120 min at 26 °C, denaturated at 95 °C for 20 min to release the complementary DNA strand which then serves as the DNA template in cross-catalysis. Consequently, after denaturation, two more DNA replicators are added that are complementary to the DNA product and contain the destabilizing abasic group. To overcome the limitations to detecting lower concentrations of RNA, namely that at low concentrations of template the templated reaction cannot be discriminated from the background-triggered reaction without any RNA template, we applied the same strategy used in the DNA-templated amplification system of decreasing the concentration of DNA replicators. Figure 3.8B illustrates how 1.4 nM of RNA template can be detected at a lower concentration of replicators (1 equiv = 1.05 μM).

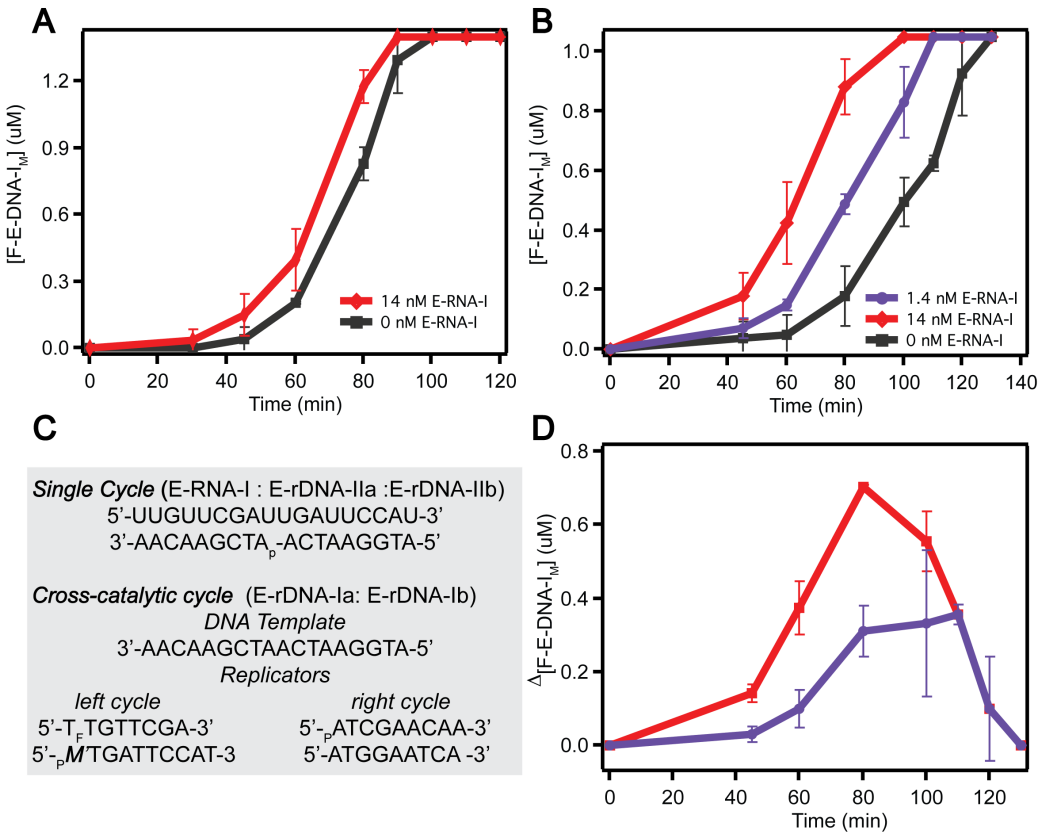

Figure 3.8 RNA-initiated LIDA with different replicator concentrations. (A) Cross-catalytic DNA amplification initiated with RNA (E-RNA-I) at higher strand concentrations (1 equiv = 1.4 μM) (B) Cross-catalytic DNA amplification initiated with RNA (E-RNA-I) at various concentrations at the lower strand concentrations (1 equiv = 1.05 μM). (C) Sequences corresponding to the first step of RNA-templated formation of cDNA (*Single Cycle*) and the second step of cross-catalytic DNA amplification (*Cross-catalytic Cycle*). (D) Difference in DNA product (ΔF-E-DNA-I$_M$) formed between the reaction initiated with 14 or 1.4 nM and 0 nM E-RNA-I. *Experimental conditions:* 14 nM, 1.4 nM or 0 nM E-RNA-I; 2 equiv E-rDNA-IIa; 2 equiv E-rDNA-IIb; 2 equiv rDNA-Ib (*M* = *Ab*); 1 equiv rDNA-Ia; *Single Cycle* performed at 26 °C for 2 hours and *Cross-Catalytic Cycle* performed at 37 °C. Experiments were performed at least two times. The reported values and error are the average and standard deviation, respectively.

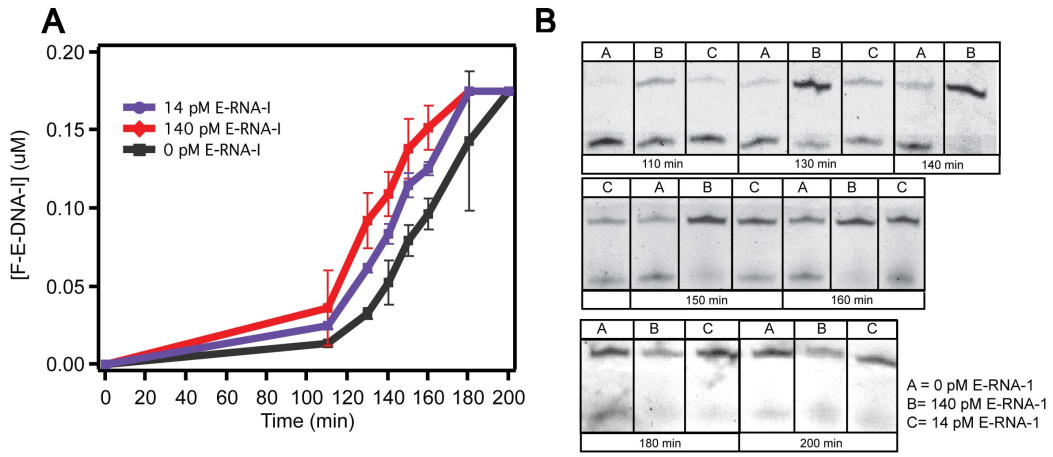

Figure 3.9 The cross-catalytic reaction of DNA for detection of RNA with lower concentration of replicators. (a) Cross-catalytic reaction initialed with RNA. The RNA initiates the ligation between two DNA replicators. The ligation products serve as a DNA template for the cross-catalytic reaction. *Experimental conditions:* 140, 1.4 or 0 pM E-RNA; 0.7 µM E-rDNA-IIa; 0.7 µM E-rDNA-IIb; 0.7 µM rDNA-Ib (*M* = *Ab*); 0.35 µM rDNA-Ia; The RNA-templated DNA at 26 °C and followed by cross-catalytic reaction at 37 °C. (b) Representative gel image corresponding to the experiment shown in (a).

To quantify the amount of self-replication, we measured the difference in fluorescent template formed between the target-initiated and background reactions (**ΔF-E-DNA-I$_M$**), as shown in Figure 3.8C. The maximum difference was then divided by the initial template concentration to yield the net number of target-initiated self-replication cycles. For example, the 14 nM **E-DNA-I** template-initiated reaction leads to 50 ± 1 replication cycles and reactions initiated with 1.4 nM template led to net replication cycles of 256 ± 20.

. Another experiment was performed further decreasing the replicator concentration. A much-reduced background reaction is therefore achieved, extending the RNA detection range to 14 pM (Figure 3.9). The lower detection limit is achieved likely because the rate of the background blunt-end reaction is

reduced with the decreasing concentration of replicators more so than the template-initiated reaction. Figure 3.9A shows that the reaction initiated with a 140 pM and 14 pM template can be distinguished from their background reactions and leads to 854 ± 302 and 5210 ± 2280 replication cycles, respectively.

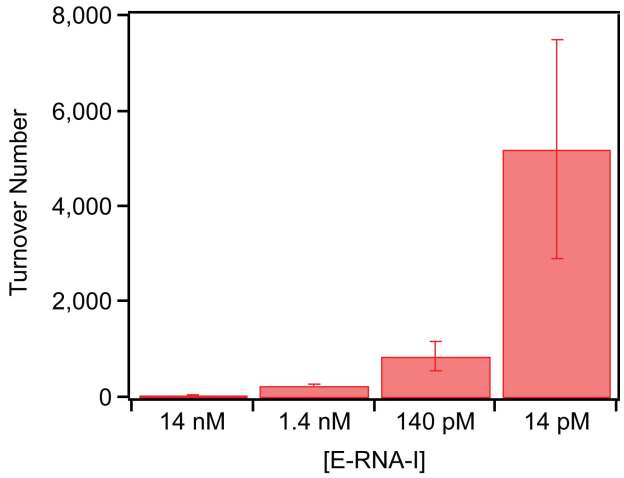

Figure 3.10 The Turnover number of F-E-DNA-I_M with ligation initiated with 14 nM, 1.4 nM, 140 pM and 14 pM E-RNA-I. The condition of replicators for 14 nM and 1.4 nM remains the same: 2.1 µM E-rDNA-IIa; 2.1 µM E-rDNA-IIb; 2.1 µM equiv rDNA-Ib (*M* = *Ab*); 1.05 µM rDNA-Ia;. The condition of replicators for 140 pM and 14 pM remains the same: 0.7 µM E-rDNA-IIa; 0.7 µM E-rDNA-IIb; 0.7 µM rDNA-Ib (*M* = *Ab*); 0.35 µM rDNA-Ia; The RNA-templated DNA at 26 °C and followed by cross-catalytic reaction at 37 °C.

3.4.3 Conclusion

In summary, a RNA detection system that incorporates lesion-induced isothermal DNA amplification was developed. Unlike other RNA-initiated amplification processes like RT-PCR, this system provides for RNA detection with one enzyme (T4 DNA ligase) with a sensitivity of 14 pM. Moreover, this system was found to be optimized at 26 °C for the RNA-templated DNA ligation step and at 37 °C for the LIDA step.

3.5 Outlook

Replacing one nucleotide with an abasic group in an 18-base sequence can alter the recognition properties of DNA. This allows it to self-replicate in a ligase chain reaction. LIDA system could potentially used as a very efficient and simple technology to amplify and detect DNA bases in general. It can be accomplished in one step with T4 DNA ligase isothermally.

As such, this system offers new possibilities in the development of isothermal RNA detection. However, there are a number of challenges that need to be overcome for effective employ LIDA to RNA detection. Such as minimizing the experimental steps and conditions, the possibility of conducting the RNA-templated DNA ligation at 37 $^{\circ}$C and denaturing the RNA-DNA hybrid by using strand displacement can be further investigated. In this regard, using RNA ligase 2 to conduct the RNA-tempalted DNA ligation with the abasic incorporated to the DNA could also be considered in future experiments.[23] The next major challenge is to significantly reduce the rate of non-templated initiated reaction. Such as optimizing the ligation buffer composition, an alternative to do this, RNA-initiated LIDA through chemical ligation are great of interest.[24]

3.6 Reference

1. Kausar, A.; Mitran, C. J.; Li, Y.; Gibbs-Davis, J. M., *Angew.Chem. Int. Edit.* **2013**, DOI: 10.1002/anie.201303225.

2. Versalovic, J.; Lupski, J. R., *Trends Microbiol.* **2002,** *10* (10), S15-S21.

3. Croce, C. M.; Calin, G. A., *Cell* **2005,** *122* (1), 6-7.

4. Coll, P.; Garrigo, M.; Moreno, C.; Marti, N., *Int. J. Tuberc. Lung D.* **2003,** *7* (9), 886-891.

5. Teles, F. R. R.; Fonseca, L. R., *Talanta* **2008,** *77* (2), 606-623.

6. Spencer, S. M.; Lin, L. N.; Chiang, C. F.; Peng, Z. C.; Hesketh, P.; Salon, J.; Huang, Z., *Chembiochem* **2010,** *11* (10), 1378-1382.

7. Epstein, J. R.; Biran, I.; Walt, D. R., *Anal. Chim. Acta* **2002,** *469* (1), 3-36.

8. Kausar, A.; McKay, R. D.; Lam, J.; Bhogal, R. S.; Tang, A. Y.; Gibbs-Davis, J. M., *Angew.Chem. Int. Edit.* **2011,** *50* (38), 8922-8926.

9. Liang, Y.; Ridzon, D.; Wong, L.; Chen, C. F., *Bmc Genomics* **2007,** *8*.

10. Ando, T.; Shishido, K., *Nihon rinsho. Japn. J. Chin. Med.* **1982,** *40* (8).

11. Chen, C. Z., *New Engl. J. Med.* **2005,** *353* (17), 1768-1771.

12. Zhang, B. H.; Pan, X. P.; Cobb, G. P.; Anderson, T. A., *Dev. Biol.* **2007,** *302* (1), 1-12.

13. Aldea, C.; Alvarez, C. P.; Folgueira, L.; Delgado, R.; Otero, J. R., *J. Clin. Microbiol.* **2002,** *40* (3), 1060-1062.

14. Yamamura, S.; Yatsushiro, S.; Yamaguchi, Y.; Abe, K.; Shinohara, Y.; Kataoka, M., *Sensors* **2012,** *12* (6), 7576-7586.

15. Wegman, D. W.; Krylov, S. N., *Trac-Trend. Anal. Chem.* **2013,** *44*, 121-130.

16. Lao, K. Q.; Xu, N. L.; Yeung, V.; Chen, C. F.; Livak, K. J.; Straus, N. A., *Biochem. Bioph. Res. Co.* **2006,** *343* (1), 85-89.

17. Liu, C. G.; Calin, G. A.; Meloon, B.; Gamliel, N.; Sevignani, C.; Ferracin, M.; Dumitru, C. D.; Shimizu, M.; Zupo, S.; Dono, M.; Alder, H.; Bullrich, F.; Negrini, M.; Croce, C. M., *P. Natl. Acad. Sci.USA.* **2004,** *101* (26), 9740-9744.

18. Chang, C. C.; Chen, C. C.; Wei, S. C.; Lu, H. H.; Liang, Y. H.; Lin, C. W., *Sensors* **2012,** *12* (6), 8319-8337.

19. Weiss, B.; Live, T. R.; Richards.Cc, *J. Biol. Chem.* **1968,** *243* (17), 4530-&.

20. Luther, A.; Brandsch, R.; von Kiedrowski, G., *Nature* **1998,** *396* (6708), 245-248.

21. Rossi, R.; Montecucco, A.; Ciarrocchi, G.; Biamonti, G., *Nucleic Acids Res.* **1997,** *25* (11), 2106-2113.

22. Higgins, N. P.; Cozzarelli, N. R., *Method. Enzymol.* **1979,** *68*.

23. Bullard, D. R.; Bowater, R. P., *Biochem. J.* **2006,** *398*, 135-144.

24. Abe, H.; Kondo, Y.; Jinmei, H.; Abe, N.; Furukawa, K.; Uchiyama, A.; Tsuneda, S.; Aikawa, K.; Matsumoto, I.; Ito, Y., *Bioconjugate Chem.* **2008,** *19* (1), 327-333.